https://doi.org/10.1093/plcell/koad061 THE PLANT CELL 2023: 35: 2369–2390

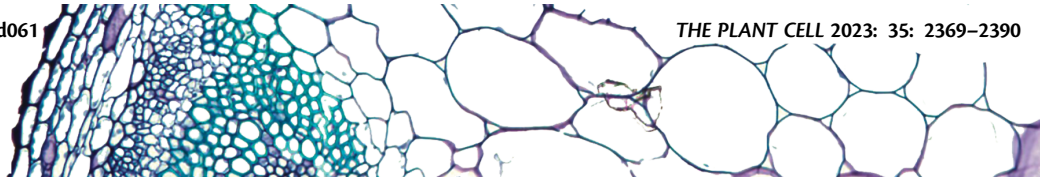

Research Article

The maize ZmVPS23-like protein relocates the nucleotide-binding leucine-rich repeat protein Rp1-D21 to endosomes and suppresses the defense response

Yang Sun,[1] Shijun Ma,[1] Xiangguo Liu[2] and Guan-Feng Wang[1,*]

1 The Key Laboratory of Plant Development and Environmental Adaptation Biology, Ministry of Education, School of Life Sciences, Shandong University, Qingdao, Shandong 266237, China
2 Institute of Agricultural Biotechnology, Jilin Academy of Agricultural Sciences, Changchun 130033, Jilin, China

*Author for correspondence: gfwang@sdu.edu.cn
The author responsible for distribution of materials integral to the findings presented in this article in accordance with the policy described in the Instructions for Authors (https://academic.oup.com/plcell/) is: Guan-Feng Wang (gfwang@sdu.edu.cn).

Abstract

Plants often utilize nucleotide-binding leucine-rich repeat (NLR) proteins to perceive pathogen infections and trigger a hypersensitive response (HR). The endosomal sorting complex required for transport (ESCRT) machinery is a conserved multisubunit complex that is essential for the biogenesis of multivesicular bodies and cargo protein sorting. VPS23 is a key component of ESCRT-I and plays important roles in plant development and abiotic stresses. *ZmVPS23L*, a homolog of *VPS23-like* in maize (*Zea mays*), was previously identified as a candidate gene in modulating HR mediated by the autoactive NLR protein Rp1-D21 in different maize populations. Here, we demonstrate that ZmVPS23L suppresses *Rp1-D21*-mediated HR in maize and *Nicotiana benthamiana*. Variation in the suppressive effect of HR by different *ZmVPS23L* alleles was correlated with variation in their expression levels. ZmVPS23 also suppressed *Rp1-D21*-mediated HR. ZmVPS23L and ZmVPS23 predominantly localized to endosomes, and they physically interacted with the coiled-coil domain of Rp1-D21 and mediated the relocation of Rp1-D21 from the nucleo-cytoplasm to endosomes. In summary, we demonstrate that ZmVPS23L and ZmVPS23 are negative regulators of *Rp1-D21*-mediated HR, likely by sequestrating Rp1-D21 in endosomes via physical interaction. Our findings reveal the role of ESCRT components in controlling plant NLR-mediated defense responses.

Introduction

Plants have evolved a sophisticated immune system to defend against pathogen infections and consist of two interconnected responses: pathogen-associated molecular pattern–triggered immunity (PTI) and effector-triggered immunity (ETI) (Jones and Dangl 2006). In PTI, plants utilize pattern recognition receptors (PRR) to perceive conserved microbial molecules termed pathogen-associated molecular patterns (PAMPs) to trigger immunity. In ETI, plants employ dominant resistance (R) proteins to detect effectors secreted from pathogens and often induce a hypersensitive response (HR), a rapid programmed cell death localized at the site of pathogen penetration. PTI and ETI act synergistically to establish a stronger disease resistance than either alone due to their mutual potentiation (Ngou et al. 2021; Yuan et al. 2021). Most R proteins carry nucleotide-binding leucine-rich repeat (NB-LRR) domains and are known as NLR proteins (Kourelis and van der Hoorn 2018). Canonical NLR proteins harbor three domains: a coiled-coil (CC) domain or a Toll/interleukin 1 receptor (TIR) domain at their N termini, a nucleotide-binding (NB)-ARC (APAF1, some *R* gene products, and CED-4) domain in the center of the protein, and an LRR domain at their C termini (Dangl and Jones 2001; Qi and Innes

Received October 06, 2022. Accepted February 28, 2023. Advance access publication March 3, 2023

2013). In the absence of pathogens, the activity of NLRs is inhibited by intra- or intermolecular interactions (Bent and Mackey 2007). Upon perception of effectors, these interactions are disrupted and trigger ETI. In some cases, such as mutations, intragenic recombination, or hybrid incompatibility, these inhibitory interactions are perturbed, causing inappropriate and spontaneous activation of NLRs in the absence of their cognate effectors (Bomblies and Weigel 2007). Plants carrying auto-active NLRs are characterized by a dwarf stature and spontaneous lesion formation (Chakraborty et al. 2018; Balint-Kurti 2019). Owing to their constitutive activation of defense responses, this type of autoimmune plants is often regarded as efficient tools for exploring novel defense regulators.

The maize (*Zea mays*) *Rp1* locus contains a cluster of tandemly repeated NLR-encoding genes that confer race-specific resistance to the fungus *Puccinia sorghi*, the causal agent of common rust (Hu et al. 1996; Hulbert 1997). The *HRp1-D* haplotype of this locus comprises *Rp1-D*, which encodes a CC-NLR protein conferring resistance to common rust, and eight paralogs designated *Rp1-dp1 to Rp1-dp8* with no known function (Sun et al. 2001). Intragenic recombination between *Rp1-D* and *Rp1-dp2* generated a novel variant *Rp1-D21* (Sun et al. 2001; Smith et al. 2010). Maize lines carrying *Rp1-D21* confer nonspecific resistance to *P. sorghi* and several nonhost species of rust (Hu et al. 1996; Smith et al. 2010). They also exhibit autoimmune phenotypes, including HR lesions and growth retardation in the absence of pathogens (Smith et al. 2010). The severity of the HR conferred by *Rp1-D21* is dependent on the genetic background, temperature, and developmental stages (Chintamanani et al. 2010). In addition, typical characteristics of HR, including the accumulation of reactive oxygen species (ROS) and the enhanced expression of defense marker genes, such as *pathogenesis-related 1* (*PR1*) and *PR5*, were also observed in *Rp1-D21* plants (Chintamanani et al. 2010).

Several studies using genome-wide association studies (GWAS) and/or quantitative trait locus (QTL) mapping approaches have identified genomic regions or loci associated with variation in the strength of Rp1-D21-mediated HR in different populations (Chintamanani et al. 2010; Olukolu et al. 2013, 2014). Based on these studies, several genes have been identified as candidate causal genes controlling this variation, including *hydroxycinnamoyltransferase (HCT)* and *caffeoyl-CoA O-methyltransferase (CCoAOMT)*, which encode two enzymes of the lignin biosynthesis pathway. These genes were functionally verified as negative regulators of Rp1-D21-mediated HR using an ectopic transient overexpression system in *Nicotiana benthamiana* (Wang et al. 2015a; Wang and Balint-Kurti 2016) and a virus-induced gene silencing system in maize (Murphree et al. 2020).

The endosomal sorting complex required for transport (ESCRT) machinery is a conserved multisubunit complex that is essential for the biogenesis of multivesicular bodies (MVBs) and the sorting of cargo proteins for degradation in the vacuole or lysosome (Gao et al. 2017; Gatta and Carlton 2019). In addition to its canonical role of sorting cargo proteins for degradation, ESCRT is also involved in sequestration of cytosolic proteins in MVBs to modulate signal transduction (Taelman et al. 2010; Szymanska et al. 2018). The ESCRT complex contains five sub-complexes, comprising ESCRT-0 (in yeast [*Saccharomyces cerevisiae*] and animals) or TOM1-like (TOL, in plants) proteins; ESCRT-I, ESCRT-II, and ESCRT-III proteins; and vacuolar protein sorting 4 (VPS4, also named suppressor of K^+ transport growth defect 1 [SKD1]) (Gao et al. 2017; Otegui 2018). ESCRT-0 or TOL recognizes ubiquitinated cargo and subsequently recruits ESCRT-I and ESCRT-II to concentrate the cargo proteins and initiate membrane remodeling. ESCRT-II then activates ESCRT-III, which mediates membrane invagination and formation of intraluminal vesicles (ILVs). The cargo proteins are incorporated in ILVs inside MVBs and ultimately degraded after the fusion of MVBs with the vacuole or lysosome (Gao et al. 2017; Gatta and Carlton 2019). In yeast and animals, the ESCRT-I complex contains four subunits, VPS23 (also named tumor susceptibility gene-101 [TSG101]), VPS28, VPS37, and MVB sorting factor of 12 kD (MVB12). The *Arabidopsis* (*Arabidopsis thaliana*) genome carries two copies of *VPS23* (*AtVPS23A* and *AtVPS23B*), *VPS28* (*AtVPS28-1* and *VPS28-2*), and *VPS37* (*AtVPS37-1* and *VPS37-2*), respectively, and the unique component *FYVE domain protein required for endosomal sorting 1* (*FREE1*), but lacks *MVB12* (Gao et al. 2017). AtVPS23A (also named ELCH [AtELC]) was reported to modulate cytokinesis via the microtubule cytoskeleton (Spitzer et al. 2006). AtVPS23A also mediates abscisic acid (ABA) signaling by interacting with the ABA receptors pyrabactin resistance 1 (PYR1)/PYR1-likes (PYLs) and regulating their vacuolar degradation (Yu et al. 2016). Interaction of AtVPS23A with the E3 ligases XB3 ortholog 5 in *Arabidopsis* thaliana 35 (XBAT35) and seven in absentia of *Arabidopsis* (SINATs) and the deubiquitinases ubiquitin-specific protease 12 (UBP12) and UBP13 affects the stability of AtVPS23A via both the proteasome and vacuolar degradation pathways, thereby regulating the abundance of ABA receptors (Xia et al. 2020; Yu et al. 2020; Liu et al. 2022). Recently, AtVPS23A was reported to be vital for salt tolerance through physical interaction with salt overly sensitive 2 (SOS2) and SOS3 and subsequent sorting of SOS2 to the plasma membrane (Lou et al. 2020). The ESCRT-I components VPS37 and VPS28 play important functions in PTI responses. For instance, AtVPS37 was found to interact with the PRR flagellin-sensitive 2 (FLS2) and mediate the sorting of FLS2 into the lumen of MVBs. Both AtVPS37 and AtVPS28 are essential for resistance to the bacterium *Pseudomonas syringae* pv. *tomato* DC3000 (*Pto* DC3000), which depends on stomatal closure (Spallek et al. 2013). However, VPS23 has not previously been implicated in the control of plant immunity, and a relationship between plant ESCRT-I components and NLR-mediated immunity has not been demonstrated.

From previous GWAS and QTL analyses, *ZmVPS23L*, a *VPS23-like* gene in maize, was identified as a major candidate gene associated with *Rp1-D21*-mediated HR (Chintamanani et al. 2010; Olukolu et al. 2013, 2014). In this study, we

demonstrate that ZmVPS23L and its homolog ZmVPS23 suppress *Rp1-D21*-mediated HR in maize and *N. benthamiana*. The expression levels of *ZmVPS23L* were largely negatively correlated with the strength of *Rp1-D21*-mediated HR. ZmVPS23L and ZmVPS23 predominantly localized on endosomes and physically interacted with the CC domain of Rp1-D21 (CC_{D21}), which promoted the relocation of Rp1-D21 from the nucleo-cytoplasm to endosomes. In summary, we show that ZmVPS23L negatively modulates HR mediated by the autoactive NLR protein Rp1-D21, likely by changing its subcellular localization via physical interaction.

Results

ZmVPS23L is a candidate regulator of *Rp1-D21*-mediated HR and partially suppresses HR in *N. benthamiana*

Three maize mapping populations have been utilized to identify regulators of Rp1-D21-mediated HR (Chintamanani et al. 2010; Olukolu et al. 2013, 2014). The same locus on chromosome 10 was repeatedly detected in different populations, as summarized in Fig. 1A. Of the six HR-associated single nucleotide polymorphisms (SNPs) detected by GWAS from a maize diversity panel (Olukolu et al. 2013), three were located within a major QTL identified from the intermated B73 × Mo17 (IBM) population (Chintamanani et al. 2010). Among these three SNPs, SNP: 21693685 was located within the coding region of GRMZM2G059010 (*DNA polymerase alpha subunit B*, *POLA*), SNP: 21722883 was located within the coding region of GRMZM2G001500 (*heat shock protein 70*, *Hsp70*) and 32.2 kb upstream of GRMZM2G348695 (no annotation, designated as *8695*), and SNP: 21823409 was located 2.1 kb upstream of GRMZM2G109582 (a *VPS23-like* gene in maize, designated as *ZmVPS23L*, see below) (Fig. 1A). Of the 44 SNPs identified from GWAS (Olukolu et al. 2014), 2 SNPs, SNP: 21804495 and SNP: 21788845, localized 15.7 kb and 31.3 kb downstream of *ZmVPS23L*, respectively, and 11.2 kb upstream and 4.1 kb downstream of AC198929.2_FG002 (no annotation, designated as 1989) (Fig. 1A). From our previous transcriptome deep sequencing (RNA-seq) analysis (Wang and Balint-Kurti 2016; Ge et al. 2021), we determined that *POLA* and *ZmVPS23L* are significantly upregulated 7 and 10 times, respectively, in the line carrying *Rp1-D21* compared to its corresponding isogenic wild-type B73, while there was no significant difference for the transcript levels of *Hsp70*, 8695 or 1989.

Agrobacterium-mediated transient expression in *N. benthamiana* is a common method to study the HR mediated by NLRs from different plant species (Padmanabhan et al. 2013; Cesari et al. 2016; Deng et al. 2017; Qi et al. 2018); we therefore used this system to investigate the role of the candidate regulators in *Rp1-D21*-mediated HR. To this end, we fused Rp1-D21 to a 3× hemagglutinin (HA) tag at its C terminus (Rp1-D21-HA), which confers an autoactive HR when its encoding construct is transiently expressed in *N. benthamiana* (Wang et al. 2015b). Co-expression of *HCT* suppresses *Rp1-D21*-mediated HR, whereas co-expression of *ß-glucuronidase* (*GUS*) has no obvious effect on *Rp1-D21*-mediated HR (Wang et al. 2015a, 2015b). We therefore used *HCT* and *GUS* as positive and negative controls, respectively. The different candidate regulators were fused to enhanced green fluorescent protein (EGFP) tag at their C termini, and the encoding constructs were co-expressed with *Rp1-D21-HA* in *N. benthamiana*. We observed that ZmVPS23L partially suppressed Rp1-D21-mediated HR, whereas other proteins (Hsp70, POLA, 8695, 1989) had no obvious effect on Rp1-D21-mediated HR (Fig. 1B). Consistent with the visual observation, ZmVPS23L significantly decreased the levels of ion leakage conductivity compared to GUS, but its effect was more modest than that of HCT, whereas other candidate proteins had no effect on ion leakage (Fig. 1B). We investigated the protein levels of Rp1-D21 and the candidate proteins by immunoblotting. Rp1-D21 abundance was largely comparable when co-expressed with different constructs encoding each candidate protein (Fig. 1B), indicating that these proteins do not affect the protein accumulation of Rp1-D21.

Rp1-D21 contains three major domains: an N-terminal CC_{D21} domain, a middle NB-ARC domain, and a C-terminal LRR domain (Wang et al. 2015b). CC_{D21} is sufficient to cause an autoactive HR when fused to an EGFP tag (CC_{D21}-EGFP) at its C terminus, and the encoding construct is transiently expressed in *N. benthamiana*. We thus used CC_{D21}-EGFP in some of the subsequent experiments owing to its higher protein abundance than Rp1-D21 according to our previous studies (Wang et al. 2015b; Wang and Balint-Kurti 2016). To investigate whether the candidate regulators affected CC_{D21}-EGFP-mediated HR, we co-expressed each with *CC_{D21}-EGFP* in *N. benthamiana*. Similar to the results of *Rp1-D21*-mediated HR, we observed that ZmVPS23L, but not the other proteins (Hsp70, POLA, 8695, 1989), partially suppresses CC_{D21}-mediated HR (Fig. 1C). These data indicate that the *ZmVPS23L* gene might be the causal gene for the regulation of *Rp1-D21*-mediated HR.

Overexpression of *ZmVPS23L* partially suppresses *Rp1-D21*-mediated HR in maize

To investigate whether ZmVPS23L modulates *Rp1-D21*-mediated HR in maize, we generated maize transgenic lines that overexpress ZmVPS23L fused to a C-terminal GFP tag in the B104 background. Six independent T1 transgenic plants were self-pollinated, and three homozygous T2 transgenic lines were obtained. Two independent T2 homozygous overexpressing lines (OE-94 and OE-98) and their corresponding nontransgenic siblings (Neg-94 and Neg-98) were crossed to the B104:*Rp1-D21* (D21 thereafter) mutant line heterozygous for *Rp1-D21* in the B104 background. The resulting F1 plants showed a 1:1 segregation ratio for *Rp1-D21*, and plants containing *Rp1-D21* had a dwarf stature and showed a lesion mimic phenotype, which can be easily identified by visual inspection. We investigated the phenotype of relevant F1 seedlings containing *Rp1-D21* grown in the field from the crosses OE-94 × D21, OE-98 × D21,

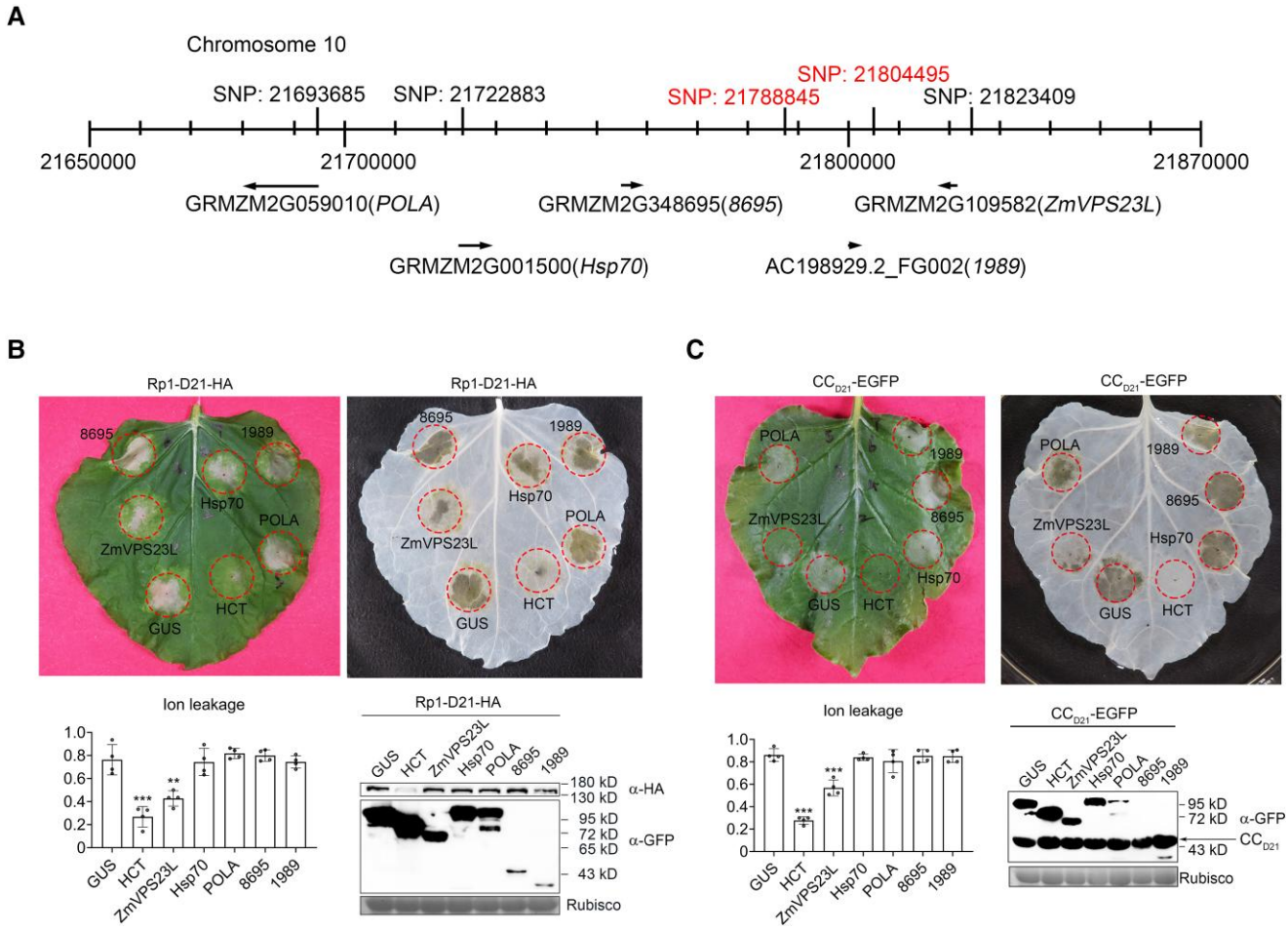

Figure 1. ZmVPS23L partially suppresses *Rp1-D21*-mediated HR in *N. benthamiana*. **A)** HR associated SNPs on chromosome 10 identified by two different mapping populations. SNPs detected by GWAS from NAM and diversity populations are shown in red and black colors, respectively. The transcription direction of the candidate genes is indicated by arrows. **B)** ZmVPS23L partially suppresses *Rp1-D21*-mediated HR in *N. benthamiana*. Constructs encoding candidate regulators fused to a C-terminal EGFP tag were transiently co-expressed with *Rp1-D21-HA* in *N. benthamiana*. The representative photograph was taken at 3 d after infiltration (dai). The same leaf cleared with ethanol is shown on the right. Ion leakage conductivity assay was carried out at 60 h after infiltration (hai). Values are means ± SD ($n = 4$ biologically independent samples). Significant difference between different samples with control *GUS* was analyzed using Student's *t* test (**$P < 0.01$, ***$P < 0.001$). Total proteins were extracted from leaves at 40 hai. Rp1-D21 was detected using an anti-HA antibody, and candidate regulators were detected with an anti-GFP antibody. Rubisco stained by Coomassie brilliant blue was used for equal loading of samples. **C)** ZmVPS23L partially suppresses CC$_{D21}$-mediated HR in *N. benthamiana*. Constructs encoding candidate regulators fused to a C-terminal EGFP tag were co-expressed with *CC$_{D21}$-EGFP* in *N. benthamiana*. The representative photograph was taken at 2 dai. The same leaf cleared with ethanol is shown on the right. Ion leakage conductivity assay was carried out at 42 hai. Values are means ± SD ($n = 4$ biologically independent samples). Significant difference between different samples with control *GUS* was analyzed using Student's *t* test (***$P < 0.001$). Total proteins were extracted from leaves at 30 hai. CC$_{D21}$ and candidate regulators were detected with an anti-GFP antibody. The arrow indicates the bands of CC$_{D21}$. Rubisco stained by Coomassie brilliant blue was used for equal loading of samples. The experiments were performed three times with similar results.

Neg-94 × D21, and Neg-98 × D21. At the V6 stage, Neg-94 × D21 and Neg-98 × D21 F1 plants showed very clear HR lesions on the new leaves (the 6th and 7th leaves), and the lesion phenotype was more obvious in older leaves, most of which even died (the 1st, 2rd, and 3rd leaves; Fig. 2A). However, in OE-94 × D21 and OE-98 × D21 F1 plants, the lesion phenotype was weak on the new leaves and much milder on the old leaves compared to the same leaves from their corresponding nontransgenic siblings (Fig. 2A). Especially in OE-94 × D21, the older leaves showed lesions but were still green and did not die (Fig. 2A). At the tasseling stage (VT), we measured plant height of the four sets of F1 plants and determined that the F1 plants from the two overexpressing lines (OE-94 × D21 and OE-98 × D21) are significantly taller than their corresponding nontransgenic siblings (Neg-94 × D21 and Neg-98 × D21), especially between OE-94 × D21 and Neg-94 × D21 (Fig. 2B). Importantly, the height of *ZmVPS23L*-OE plants not crossed to B104:*Rp1-D21* was similar to that of the corresponding nontransgenic siblings (Supplemental Fig. S1), indicating that overexpression of

ZmVPS23L per se did not affect plant height under normal growth conditions. Moreover, we measured the chlorophyll contents from the four different sets of F1 plants, which revealed higher chlorophyll contents in the F1 plants derived from the two overexpressing lines (OE-94 × D21 and OE-98 × D21) than from the corresponding nontransgenic siblings (Neg-94 × D21 and Neg-98 × D21) (Fig. 2C). To investigate whether ZmVPS23L suppression of *Rp1-D21*-mediated HR is related to *ZmVPS23L* expression levels in maize, we performed reverse transcription quantitative PCR (RT-qPCR) and immunoblotting assays. *ZmVPS23L* transcript levels in OE-94 × D21 and OE-98 × D21 F1 plants were 62 and 4 times higher than Neg-94 × D21 and Neg-98 × D21 F1 plants, respectively (Fig. 2D). Consistently, ZmVPS23L was more abundant in OE-94 × D21 F1 plants compared to that in OE-98 × D21 F1 plants, as determined by immunoblotting with an anti-GFP antibody (Fig. 2E). The defense marker genes *PR1* and *PR5* are upregulated in *Rp1-D21* compared to wild type (Chintamanani et al. 2010). By contrast, we detected lower transcript levels for *PR1* and *PR5* in the F1 plants for the two *ZmVPS23L* overexpression lines carrying *Rp1-D21* compared to their nontransgenic siblings (Fig. 2F). Taken together, these results indicate that ZmVPS23L significantly suppresses Rp1-D21-mediated HR in maize, and *ZmVPS23L* expression levels are related to the strength of suppression of the HR phenotype in maize carrying *Rp1-D21*.

Maize homozygous for *Rp1-D21* cannot produce a viable ear owing to its strong autoimmune responses (Chintamanani et al. 2010); therefore, *Rp1-D21* was maintained as a heterozygous state in most genetic backgrounds. Due to the strong inhibition effect of ZmVPS23L on *Rp1-D21*-mediated HR in the F1 generation, we were able to self-pollinate OE-94 × D21 and OE-98 × D21 F1 plants to obtain two F2 populations. To confirm the role of ZmVPS23L on *Rp1-D21*-mediated HR, we investigated the phenotype of seedlings in the two F2 populations. Because we are not able to differentiate the homozygous state of *ZmVPS23L* from the heterozygous state, we classified the F2 population into four groups: plants without *ZmVPS23L-GFP* or *Rp1-D21* (named as VPS23L$^-$D21$^-$), plants overexpressing *ZmVPS23L-GFP* but without *Rp1-D21* (VPS23L$^+$D21$^-$), plants carrying *Rp1-D21* but without ZmVPS23L-GFP (VPS23L$^-$D21$^+$), and plants carrying both *ZmVPS23L-GFP* and *Rp1-D21* (VPS23L$^+$D21$^+$). The protein levels of ZmVPS23L in F2 population were detected by immunoblot analysis with an anti-GFP antibody to identify plants harboring *ZmVPS23L-GFP* (Supplemental Fig. S2A). We obtained 35 individual plants of the F2 population from OE-94 × D21, consisting of 3 VPS23L$^-$D21$^-$, 5 VPS23L$^+$D21$^-$, 6 VPS23L$^-$D21$^+$, and 21 VPS23L$^+$D21$^+$ plants. We obtained 57 individual plants of the F2 population from OE-98 × D21, with 6 VPS23L$^-$D21$^-$, 13 VPS23L$^+$D21$^-$, 4 VPS23L$^-$D21$^+$, and 34 VPS23L$^+$D21$^+$ plants. Regardless of the presence of VPS23L-GFP, plants without *Rp1-D21* (VPS23L$^-$D21$^-$ and VPS23L$^+$D21$^-$) showed similar phenotypes without HR lesions (Supplemental Fig. S2B). However, VPS23L$^-$D21$^+$ plants in the F2 population displayed strong lesions, while VPS23L$^+$D21$^+$ plants exhibited significantly weaker lesions (Supplemental Fig. S2B). Height was not affected by *ZmVPS23L-GFP* in F2 plants without *Rp1-D21*, while the height of VPS23L$^+$D21$^+$ plants was significantly higher than that of the VPS23L$^-$D21$^+$ plants (Supplemental Fig. S2C).

Mutation of *ZmVPS23L* enhances *Rp1-D21*-mediated HR in maize

To verify the role of *ZmVPS23L* in *Rp1-D21*-mediated HR in maize, we obtained a heterozygous mutant line for *ZmVPS23L* with an *Ac/Ds* transposon insertion at 229 bp downstream of ATG (Supplemental Fig. S3A), designed as *Zmvps23l*. We allowed the heterozygous plant to self-pollinate to get homozygous *Zmvps23l* and wild-type (WT) siblings (Supplemental Fig. S3B). *ZmVPS23L* transcript level was significantly decreased in the *Zmvps23l* homozygous line compared to WT plants (Supplemental Fig. S3C). We crossed the maize line A632 heterozygous for *Rp1-D21* (A632:*Rp1-D21*) to the *Zmvps23l* homozygous line, followed by two backcrosses of the F1 plants heterozygous *Rp1-D21* to *Zmvps23l* to obtain a BC2F1 population. We grew 44 individual plants from the BC2F1 population and classified them into 4 groups based on genotyping and visual inspection of the HR phenotype (Supplemental Fig. S4): 8 plants heterozygous for *Zmvps23l* but without *Rp1-D21* (*vps23l*/*VPS23L* D21$^-$), 12 plants homozygous for *Zmvps23l* but without *Rp1-D21* (*vps23l* D21$^-$), 11 plants heterozygous for *Zmvps23l* and with *Rp1-D21* (*vps23l*/*VPS23L* D21$^+$), and 13 plants homozygous for *Zmvps23l* and with *Rp1-D21* (*vps23l* D21$^+$). The *vps23l* D21$^+$ plants displayed stronger HR lesions than *vps23l*/*VPS23L* D21$^+$ plants (Fig. 3, A to C). Plant height for *vps23l* D21$^+$ was significantly lower than that of *vps23l*/*VPS23L* D21$^+$ at the V9 stage, whereas plant height was not affected by the *Zmvps23l* mutation in plants without *Rp1-D21* (Fig. 3D). *vps23l* D21$^+$ plants accumulated significantly less chlorophyll than *vps23l*/*VPS23L* D21$^+$ plants, while *vps23l*/*VPS23L* D21$^-$ and *vps23l* D21$^-$ had no HR lesions and had similar levels of chlorophyll (Fig. 3E). By RT-qPCR, the transcript level of *ZmVPS23L* in *vps23l* D21$^+$ was significantly decreased than that in *vps23l*/*VPS23L* D21$^+$ plants (Fig. 3F). These results indicate that the loss of ZmVPS23L function enhance *Rp1-D21*-mediated HR in maize.

ZmVPS23L transcript levels are largely negatively related with HR strength in NAM parental lines containing *Rp1-D21*

According to GWAS carried out by Olukolu et al. (2013), a SNP associated with Rp1-D21-mediated HR was detected 2.1 kb upstream of *ZmVPS23L*. Combined with the data above, we speculated that *ZmVPS23L* transcript levels might be related to the strength of *Rp1-D21*-mediated HR. We analyzed the *ZmVPS23L* promoter sequences about 2.6 kb upstream of the start codon in Mo17 and 25 nested association mapping (NAM) parental lines downloaded

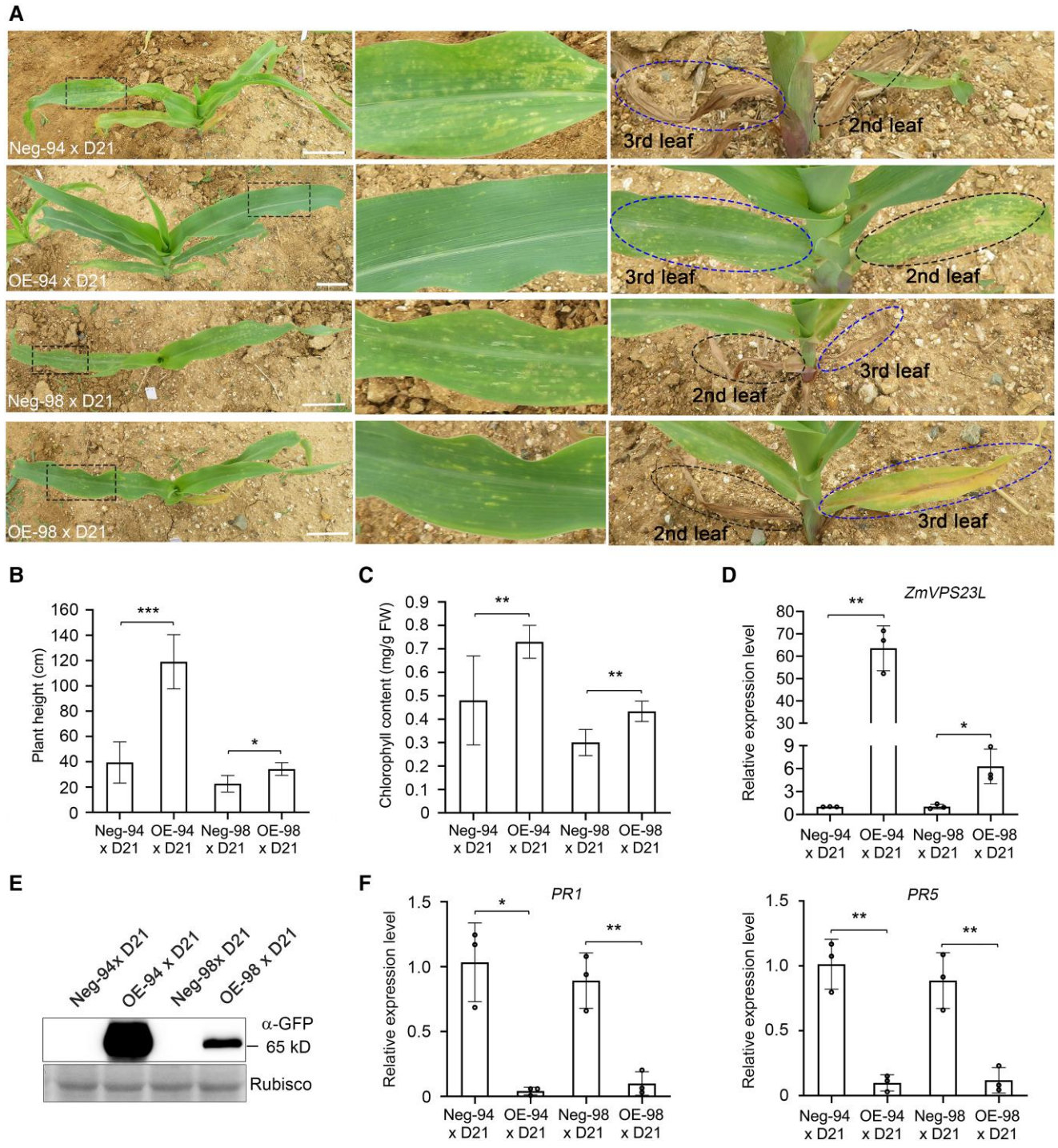

Figure 2. Overexpression of *ZmVPS23L* suppresses *Rp1-D21*-mediated HR in maize at the V6 and VT stages. **A)** ZmVPS23L suppresses leaf lesions induced by Rp1-D21 in maize. Fl plants obtained from the cross between homozygous T2 *ZmVPS23L* overexpression lines and *Rp1-D21* at the V6 stage. Images of the whole seedlings are shown on the left panel. Images of the new leaves (in the black boxes) are enlarged and shown in the middle panel. Images of older leaves are enlarged and shown on the right panel. Black and blue circles show the second and the third leaves, respectively, in different lines. Scale bars, 5 cm. **B)** ZmVPS23L suppresses the dwarf phenotype induced by *Rp1-D21* in maize. Plant heights were measured at the VT stage. Values are means ± SD ($n \geq 12$ for 94×D21, $n \geq 6$ for 98×D21). Significant difference between samples was analyzed using Student's *t* test (*$P < 0.05$, ***$P < 0.001$). **C)** Chlorophyll content is elevated in *ZmVPS23L* overexpression lines. Chlorophylls were extracted from maize leaves at the VT stage. Values are means ± SD ($n \geq 7$ for 94×D21, $n \geq 6$ for 98×D21). Significant difference between samples was analyzed using Student's *t* test (**$P < 0.01$). **D)** *ZmVPS23L* transcript levels are higher in *ZmVPS23L* overexpression lines as detected by RT-qPCR. RNA was extracted from leaves of maize seedlings at the five-leaf stage. Values are means ± SD ($n = 3$ biologically independent samples). Significant difference between samples

(continued)

from MaizeGDB (https://www.maizegdb.org/) and classified the promoter sequences into four major haplotypes (Supplemental Fig. S5). We selected seven maize lines belonging to these four haplotypes for further analysis. The severity of *Rp1-D21*-mediated HR in different genetic backgrounds was previously investigated on a 0 to 9 scale, with 0 for no HR and 9 for very severe HR (Chintamanani et al. 2010; Negeri et al. 2013). *Rp1-D21* caused the most severe HR in haplotype 1 lines (NC350 and CML322), moderate HR in haplotype 3 lines (NC358, IL14H and Mo17), and very weak HR in one haplotype 4 line (B97) and one haplotype 2 line (CML228). We investigated *ZmPR1* transcript levels in different haplotype lines harboring *Rp1-D21* and observed that *ZmPR1* is most highly expressed in haplotype 1 lines, expressed at moderate levels in haplotype 2 and 3 lines, and expressed to lowest level in the haplotype 4 line (Supplemental Fig. S6A). *ZmVPS23L* transcript level was lowest in the haplotype 1 line CML322, moderate in the haplotype 2 line CML228 and the haplotype 3 line Mo17, and highest in the haplotype 4 line B97 (Supplemental Fig. S6B). Therefore, *ZmVPS23L* transcript levels are largely in a negative relation with the HR severity mediated by *Rp1-D21*.

Different *ZmVPS23L* alleles in NAM parental lines similarly suppress *Rp1-D21*-mediated HR

To examine whether the difference in the *ZmVPS23L* coding sequence is related to its effect on HR regulation, we analyzed the *ZmVPS23L* coding sequence in Mo17 and 25 NAM parental lines downloaded from MaizeGDB (https://www.maizegdb.org/) and classified the sequence into six alleles (Supplemental Fig. S7). We cloned all six alleles of *ZmVPS23L* and upstream of *EGFP*. When co-expressed with CC_{D21}-*EGFP* in *N. benthamiana*, all 6 alleles suppressed HR to similar levels (Supplemental Fig. S8).

ZmVPS23, the homolog of ZmVPS23L also suppresses CC_{D21}-mediated HR in *N. benthamiana*

Using ZmVPS23L as a query to search the maize genome database, we identified a homolog of ZmVPS23L, GRMZM2G147579. We constructed a phylogenetic tree (Fig. 4A) and found that GRMZM2G147579 clusters in the same clade as *Arabidopsis* VPS23A and VPS23B, whereas ZmVPS23L was in the same clade as no functional annotated *Arabidopsis* At2g38830 (27% identity at the protein level). We therefore named GRMZM2G147579 as ZmVPS23. Similar to AtVPS23A and AtVPS23B, both ZmVPS23 and ZmVPS23L contained an ubiquitin-conjugating enzyme variant (UEV) domain at the N terminus, which lacks the conserved cysteine in the ubiquitin-conjugating domain, a CC domain in the center of the protein, and a VPS23 core domain (also named steadiness box) at the C terminus (Supplemental Fig. S9). Similar to *ZmVPS23L*, *ZmVPS23* also partially suppressed CC_{D21}-mediated HR when transiently co-expressed in *N. benthamiana* (Fig. 4B).

ZmVPS23L and ZmVPS23 are not general cell death suppressors

To investigate whether ZmVPS23L and ZmVPS23 are common cell death suppressors, we transiently co-expressed their encoding constructs individually with other NLR variants or cell death elicitors in *N. benthamiana*. *MLA10* and *RPM1*(D505V) (*resistance to P. syringae* pv. *maculicola 1*) are two CC-NLR genes that trigger autoactive HR when transiently expressed in *N. benthamiana* (Gao et al. 2011; Bai et al. 2012). Neither *ZmVPS23L* nor *ZmVPS23* suppressed HR induced by *MLA10* or *RPM1*(D505V) in *N. benthamiana* (Supplemental Fig. S10A). Bax is a member of the Bcl-2 family in animals; INF1 is an HR elicitor produced by *Phytophthora infestans*. Both *Bax* and *INF1* induce cell death when transiently expressed in *N. benthamiana* (Kamoun et al. 1998; Lacomme and Santa Cruz 1999). Neither *ZmVPS23L* nor *ZmVPS23* inhibited cell death induced by *Bax* or *INF1* in *N. benthamiana* (Supplemental Fig. S10B). Taken together, the above results suggest that ZmVPS23L and ZmVPS23 are not common suppressors of cell death.

Both ZmVPS23L and ZmVPS23 localize in the endosomes

VPS23 is a component of the ESCRT-I complex, which predominantly localizes to endosomes and contributes to cargo sorting in vesicle trafficking in *Arabidopsis* (Spitzer et al. 2006; Yu et al. 2016). We speculated that ZmVPS23L and ZmVPS23 might play a similar role and therefore checked their subcellular localization. We drove the expression of *ZmVPS23L*, cloned in-frame and upstream of *GFP*, from the maize *Ubiquitin* promoter: we observed a predominantly punctate localization pattern in the protoplasts prepared from maize transgenic overexpressing lines (Supplemental Fig. S11A). Similarly, *ZmVPS23L-GFP* and *ZmVPS23-GFP* driven by the cauliflower mosaic virus (CaMV) 35S promoter mainly resulted in a punctate distribution pattern when transiently expressed in maize protoplasts and in *N. benthamiana* leaves (Supplemental Fig. S11, B and S11C), reminiscent of the endosomal localization of AtVPS23 (Spitzer et al. 2006; Yu

Figure 2. (Continued)
was analyzed using Student's *t* test (*$P < 0.05$, **$P < 0.01$). **E)** Protein accumulation of ZmVPS23L investigated in *ZmVPS23L* overexpression lines, as detected by immunoblotting. Proteins were extracted from leaves of maize seedlings at the five-leaf stage. An anti-GFP antibody was used to detect ZmVPS23L. Coomassie brilliant blue (CBB) staining of Rubisco proteins was used for loading control. The transcript levels of *PRI* and *PR5* are lower in *ZmVPS23L* overexpression lines, as detected by RT-qPCR. RNA was extracted from leaves of maize seedlings at five-leaf stage. Values are means ± SD ($n = 3$ biologically independent samples). Significant difference between samples was analyzed using Student's *t* test (*$P < 0.05$, * *$P < 0.01$).

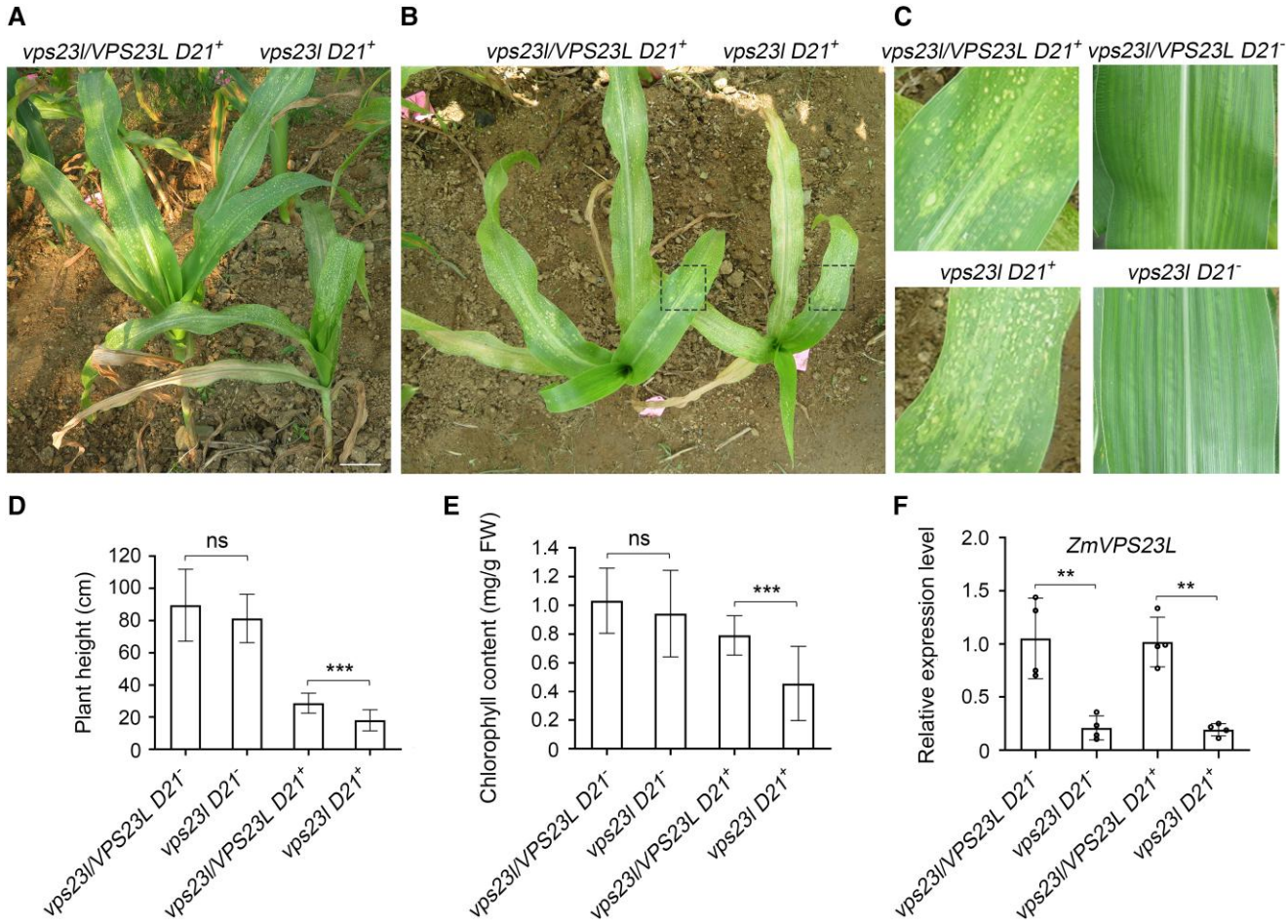

Figure 3. Mutation of *ZmVPS23L* enhances *Rp1-D21*-mediated HR in maize at the V9 stage. **A to C)** Mutation of *ZmVPS23L* enhances leaf lesions induced by *Rp1-D21* in maize. The homozygous *Zmvps23l* mutant was crossed to maize carrying *Rp1-D21*, and the F1 plants were subsequently backcrossed twice to the homozygous *Zmvps23l* mutant to obtain the BC2F1 population. Images of the whole seedlings of the BC2F1 population are shown on the left panel. Images taken from the upside were shown in the middle panel. Images of leaves in the black boxes are enlarged and shown on the right panel. Scale bars, 5 cm. **D)** Homozygous *Zmvps23l* enhances the dwarf phenotype induced by *Rp1-D21* in maize. Plant height was measured at the V9 stage. Values are means ± SD ($n \geq 8$ for D21^{-}, $n \geq 11$ for D21^{+}). Significant difference between samples was analyzed using Student's *t* test (***$P < 0.001$). **E)** Chlorophyll content is lower in homozygous *Zmvps23l* lines. Chlorophyll content was extracted from maize leaves at V9 stage. Values are means ± SD ($n \geq 8$ for D21^{-}, $n \geq 11$ for D21^{+}). Significant difference between samples was analyzed using Student's *t* test (***$P < 0.001$). **F)** *ZmVPS23L* transcript levels are significantly decreased in homozygous *Zmvps23l* lines as detected by RT-qPCR. RNA was extracted from leaves of maize seedlings at the V9 stage. Values are means ± SD ($n = 4$ biologically independent samples). Significant difference between samples was analyzed using Student's *t* test (**$P < 0.01$).

et al. 2016). To validate the above results, we cloned a 1.5 kb promoter fragment of *ZmVPS23L* and *ZmVPS23* upstream of the ATG, to generate *proZmVPS23L:ZmVPS23L-GFP* and *proZmVPS23:ZmVPS23-GFP*. When maize protoplasts were transiently transfected with these constructs, ZmVPS23L and ZmVPS23 also predominantly localized to punctate structures, as well as in the cytoplasm (Supplemental Fig. S11D). To determine which subcellular structure ZmVPS23L and ZmVPS23 localize to, we transiently co-transfected *proZmVPS23L:ZmVPS23L-GFP* or *proZmVPS23:ZmVPS23-GFP* with the early endosome marker construct *mRFP-SYP61* (*syntaxin of plants 61*) and the late endosome marker construct *mRFP-VSR2* (*vacuolar sorting receptor 2*) in maize protoplasts. We determined that ZmVPS23L and ZmVPS23 predominantly colocalize with the two endosome markers (Fig. 5A). We observed a similar colocalization pattern when *ZmVPS23L* and *ZmVPS23* were transiently expressed from the 35S promoter with the two endosome marker constructs in maize protoplasts (Supplemental Fig. S11E). To verify this result, we transiently co-infiltrated *35S:ZmVPS23L-RFP* and *35S:ZmVPS23-RFP* constructs with *SYP61-GFP* or the other late endosome marker *GFP-ARA7* in *N. benthamiana* and observed that ZmVPS23L and ZmVPS23 mainly colocalize with the early endosome marker, and only partially with the late endosome marker *GFP-ARA7* (Fig. 5B). We also determined that both ZmVPS23L and ZmVPS23 colocalize with AtVPS23A in both *N. benthamiana* leaves and maize protoplasts (Supplemental Fig. S12).

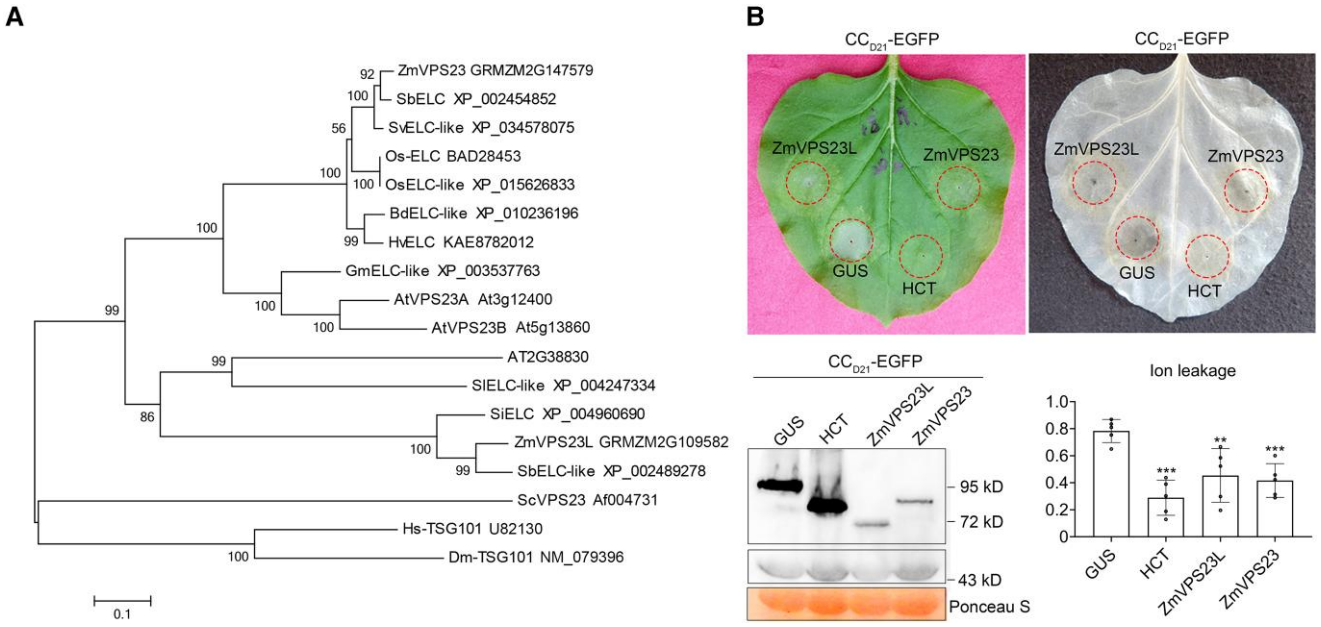

Figure 4. ZmVPS23, the homolog of ZmVPS23L, suppresses CC_{D21}-mediated HR in *N. benthamiana*. **A)** Phylogenetic analysis of VPS23 and its homologs in different plant species based on the amino acid sequences. The scale bar represents the branch length. The numbers at the nodes represent the percentage of 1,000 bootstraps. At: *Arabidopsis thaliana*; Bd: *Brachypodium distachyon*; Dm: *Drosophila melanogaster*, Gm: *Glycine max*; Hs: *Homo sapiens*; Hv: *Hordeum vulgare*; Os: *Oryza sativa*; Sb: *Sorghum bicolor*, Sc: *Saccharomyces cerevisiae*; Si: *Setaria italica*; Sl: *Solanum lycopersicum*; Sv: *Setaria viridis*; Zm: *Zea mays*. **B)** ZmVPS23 suppresses CC_{D21}-mediated HR in *N. benthamiana*. A construct encoding ZmVPS23 fused to a C-terminal EGFP tag was co-expressed with *CC_{D21}-EGFP* in *N. benthamiana*. The representative photograph was taken at 2 dai. The same leaf cleared with ethanol is shown on the right. Ion leakage conductivity assay was carried out at 40 hai. Values are means ± SD ($n = 5$ biologically independent samples). Significant difference between samples was analyzed using Student's *t* test (**$P < 0.01$, ***$P < 0.001$). Total proteins were extracted from leaves at 30 hai. Proteins were detected with an anti-GFP antibody. Rubisco stained by Ponceau S was used for equal loading of samples. The experiments were performed three times with similar results.

However, ZmVPS23L and ZmVPS23 did not colocalize with ER, Golgi, or peroxisome markers in *N. benthamiana* (Supplemental Fig. S13). These results indicate that ZmVPS23L and ZmVPS23 predominantly localize to the endosomes, and also in the cytoplasm.

ZmVPS23L promotes the subcellular localization of CC_{D21} and Rp1-D21 to endosomes

Rp1-D21 and CC_{D21} mainly localize in the cytoplasm and the nucleus, and its nucleo-cytoplasmic shuttling is believed to be required for HR induction (Wang and Balint-Kurti 2015). AtVPS23, which localizes in the endosomes and the cytoplasm, acts in vesicle trafficking (Yu et al. 2016; Gao et al. 2017; Xia et al. 2020). As homologs of AtVPS23, we speculated that ZmVPS23L and ZmVPS23 might have similar roles and affect the localization of Rp1-D21 and CC_{D21}. To test this hypothesis, we co-expressed *CC_{D21}-RFP* and *ZmVPS23L-GFP* or *ZmVPS23-GFP* under the 35S promoter in maize protoplasts, with *GUS-GFP* as control. When co-expressed with *ZmVPS23L-GFP* or *ZmVPS23-GFP*, CC_{D21} displayed punctate signals that overlap with ZmVPS23L-GFP or ZmVPS23-GFP, whereas CC_{D21} mainly localized in the cytoplasm and nucleus when co-expressed with *GUS* (Fig. 6A). To verify these results, we cloned the native promoter of *Rp1-D21* (*proD21*) and generated the *proD21:CC_{D21}-mRFP* construct and found that CC_{D21}-mRFP mainly localizes in the cytoplasm and nucleus in maize protoplasts (Fig. 6B), similar to CC_{D21}-RFP when its encoding construct is driven by the 35S promoter. When transiently co-transfected maize protoplasts with *proZmVPS23L:ZmVPS23L-GFP* or *proZmVPS23:ZmVPS23-GFP* with *proD21:CC_{D21}-mRFP*, we determined that CC_{D21} predominantly localizes to punctate structures (Fig. 6C). Transient co-infiltration of *N. benthamiana* leaves with *CC_{D21}-RFP* and *ZmVPS23L-GFP* or *ZmVPS23-GFP* driven by the 35S promoter confirmed these results (Fig. 6D). We also performed a protein fractionation assay of *N. benthamiana* leaves co-expressing *CC_{D21}-RFP* with *ZmVPS23L* or *ZmVPS23*: we established that CC_{D21}-RFP abundance increases in the microsomal fraction in the presence of with ZmVPS23L or ZmVPS23 compared to GUS (Fig. 6E and F). Intriguingly, when *CC_{D21}-RFP* and *ZmVPS23L-GFP* were co-expressed in *N. benthamiana*, several small puncta fused and formed larger protein aggregates (Supplemental Movie S1 online). We also observed that ZmVPS23L and ZmVPS23, but not GUS, change the subcellular localization of Rp1-D21 to these punctate structures (Supplemental Fig. S14).

To further investigate whether ZmVPS23L promoted the subcellular localization of CC_{D21} to endosomes, we

co-expressed CC_{D21}-*RFP*, *ZmVPS23L-CFP*, and the endosome marker *GFP-SYP61* in *N. benthamiana*. We determined that the punctate structures partially colocalize with the endosome marker (Supplemental Fig. S15), indicating that ZmVPS23L promotes the relocation of CC_{D21} to endosomes.

ZmVPS23L interacts with the CC_{D21} domain

Many proteins involved in vesicle trafficking, including AtVPS23, interact with their cargo proteins (Yu et al. 2016; Lou et al. 2020). To investigate whether ZmVPS23L or ZmVPS23 can change the subcellular localization of CC_{D21} by protein–protein interaction, we co-expressed *ZmVPS23L-EGFP* or *ZmVPS23-EGFP* with CC_{D21}-*Myc* in *N. benthamiana* and performed co-immunoprecipitation (Co-IP) assays. We previously demonstrated that HCT interacted with CC_{D21} in Co-IP assays (Wang et al. 2015a; Wang and Balint-Kurti 2016), and it was therefore used as a positive control in this study. As shown in Fig. 7A, CC_{D21} co-immunoprecipitated strongly with ZmVPS23L-GFP when using an anti-GFP antibody, which was similar to the interaction between CC_{D21} and HCT; however, ZmVPS23-GFP interacted weakly with CC_{D21}, which might be caused by the low abundance of the ZmVPS23-GFP fusion protein in this assay. To validate these interactions, we carried out a yeast two-hybrid assay and observed that ZmVPS23L associates with CC_{D21}, whereas ZmVPS23 had no or very weak interaction with CC_{D21} in yeast (Fig. 7B and Supplemental Fig. S19A). Bimolecular fluorescence complementation (BiFC) assays confirmed that ZmVPS23L and ZmVPS23 interact with CC_{D21} in punctate structures in *N. benthamiana*; these punctate signals partially colocalized with the endosome marker SYP61 (Fig. 7C and Supplemental Fig. S20A). To verify the protein interactions in a more native state, we cloned the *ZmVPS23L*, *ZmVPS23*, and CC_{D21} coding sequences into BiFC vectors driven by their native promoters. After co-transfecting these modified BiFC vectors in maize protoplasts, we determined that CC_{D21} also interacts with ZmVPS23L or ZmVPS23 in punctuate structures (Fig. 7D). Since ZmVPS23L and ZmVPS23 did not suppress MLA10-mediated HR (Supplemental Fig. S10), we speculated that it might be due to their inability to interact with the CC domain of MLA10 (CC_{MLA}). To test the hypothesis, we used yeast two-hybrid and BiFC assays: indeed, neither ZmVPS23L nor ZmVPS23 interacted with CC_{MLA} in either assay (Supplemental Figs. S16, S19C, and S20C). Taken together, the above results indicate that ZmVPS23L or ZmVPS23 promotes the relocation of CC_{D21} to the endosome, probably through protein–protein interaction.

ZmVPS23L and ZmVPS23 form homomers and heteromers

Both AtVPS23A and AtVPS23B can form dimers (Richardson et al. 2011). We therefore tested whether ZmVPS23L and ZmVPS23 can self-associate by yeast two-hybrid and BiFC assays. We observed that both ZmVPS23L and ZmVPS23 can self-associate (Supplemental Figs. S17, A, B, S19D and S20D). Moreover, ZmVPS23L interacted with ZmVPS23 (Supplemental Fig. S17, C and D). The above results indicate that ZmVPS23L and ZmVPS23 form homomers and heteromers.

We further co-expressed *ZmVPS23L* and *ZmVPS23* with CC_{D21}-*EGFP* in *N. benthamiana* and determined that they exert a stronger inhibition effect than either alone on CC_{D21}-mediated HR (Supplemental Fig. S17E).

The UEV-CC domain and the CC-VPS23 core domain of ZmVPS23L partially suppress CC_{D21}-mediated HR by interacting with CC_{D21} and relocating it to endosomes

To investigate which domains of ZmVPS23L are responsible for HR suppression and interaction with CC_{D21}, we divided ZmVPS23L into different fragments containing UEV, CC, VPS23 core, UEV-CC, or CC-VPS23 core domain and fused each to a C-terminal GFP tag (Fig. 8A). We co-expressed each construct with CC_{D21}-*EGFP* in *N. benthamiana*, which revealed that the UEV domain, CC domain, and VPS23 core domain alone do not suppress CC_{D21}-mediated HR, while the UEV-CC domain and the CC-VPS23 core domain partially suppressed the HR (Fig. 8B). We investigated the interactions between these fragments and CC_{D21}. A yeast two-hybrid assay showed that the UEV domain, the CC domain, the UEV-CC domain, and the CC-VPS23 core domain, but not the VPS23-core domain alone, physically interact with CC_{D21} (Fig. 8C and Supplemental Fig. S19B). In BiFC assays, CC_{D21} interacted with the UEV, the CC, and the VPS23 core domains, and the signals predominantly displayed a nucleo-cytoplasmic distribution (Fig. 8D and Supplemental Fig. S20B). However, CC_{D21} interacted with the UEV-CC domain and the CC-VPS23 core domain and predominantly displayed a punctate localization (Fig. 8D). These results prompted us to investigate the subcellular localization of the different ZmVPS23L domains. We found that the UEV, CC, and VPS23 core domains predominantly localize in the nucleo-cytoplasm, whereas the UEV-CC domain and the CC-VPS23 core domain predominantly localized in the punctate structures, with a weak signal in the nucleus and cytoplasm (Supplemental Fig. S18A). When co-expressed with different ZmVPS23L domains, CC_{D21} colocalized in the nucleo-cytoplasm with the UEV, CC, and VPS23 core domains, whereas it predominantly relocated to the punctuate structures with the UEV-CC and CC-VPS23 core domains (Fig. 8D and Supplemental Fig. S18B). Taken together, the UEV-CC domain and CC-VPS23 core domain of ZmVPS23L partially suppressed CC_{D21}-mediated HR likely by interacting with CC_{D21} and relocating it to endosomes.

Discussion

Rp1-D21 is a CC-NLR conferring autoimmunity in maize. Three independent studies using different mapping populations identified the same locus on chromosome 10

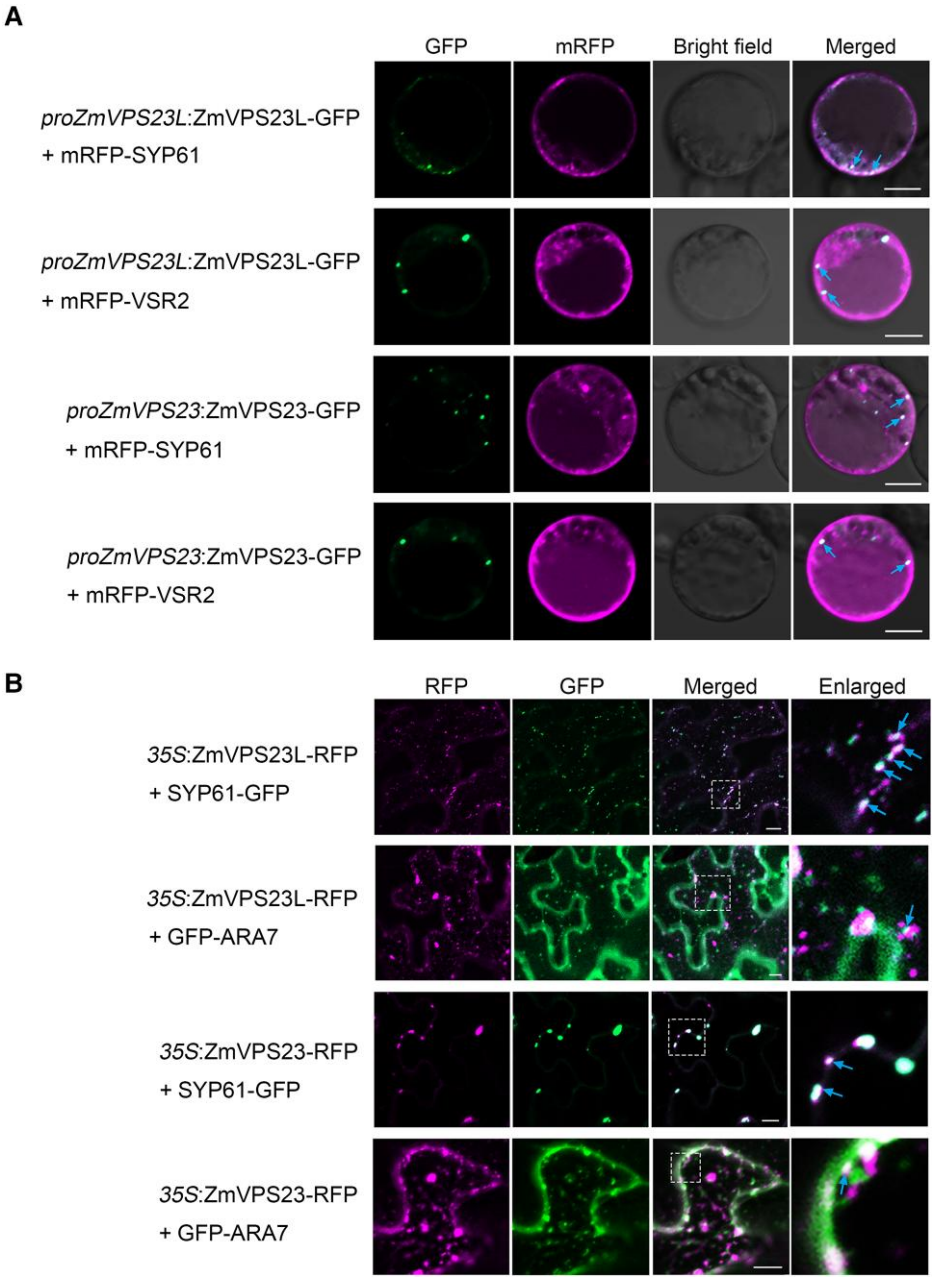

Figure 5. Investigating the subcellular localization of ZmVPS23L and ZmVPS23 in maize protoplasts and *N. benthamiana* leaves. **A)** *ZmVPS23L-EGFP* and *ZmVPS23-EGFP* driven by their native promoters were transiently co-transfected with the early endosome marker *mRFP-SYP61* or the late endosome marker *mRFP-VSR2* in maize protoplasts. Arrows indicate the colocalization of ZmVPS23L with the endosome markers. Scale bars, 10 μm. **B)** *ZmVPS23L-GFP* and *ZmVPS23-GFP* driven by the 35S promoter were transiently co-expressed with the early endosome marker *SYP61-GFP* and the late endosome marker *GFP-ARA7* in *N. benthamiana* leaves. Images in the white boxes are enlarged and shown in the right panel. Arrows indicate the colocalization of ZmVPS23L with the endosome markers. Scale bars, 10 μm.

associated with the modulation of Rp1-D21-mediated HR (Chintamanani et al. 2010; Olukolu et al. 2013, 2014). Combining this genetic analysis, *Agrobacterium*-mediated transient expression in *N. benthamiana*, and stable transgenic and mutant analyses in maize, we verified that *ZmVPS23L* was the causal gene at this locus and that it negatively modulated *Rp1-D21*-mediated HR. We further demonstrated that the transcript levels of *ZmVPS23L* in different backgrounds were largely negatively related to the HR strength. According to RNA-seq data (Christie et al. 2017; Ding et al. 2019; Yu et al. 2022), *ZmVPS23L* transcript levels were induced by *Cercospora zeina* and *Cochliobolus heterostrophus*, the causal agents of gray leaf spot and southern leaf blight in maize; *ZmVPS23L* was also differentially expressed under abiotic stresses, e.g. drought or salt. These results suggest that *ZmVPS23L* might

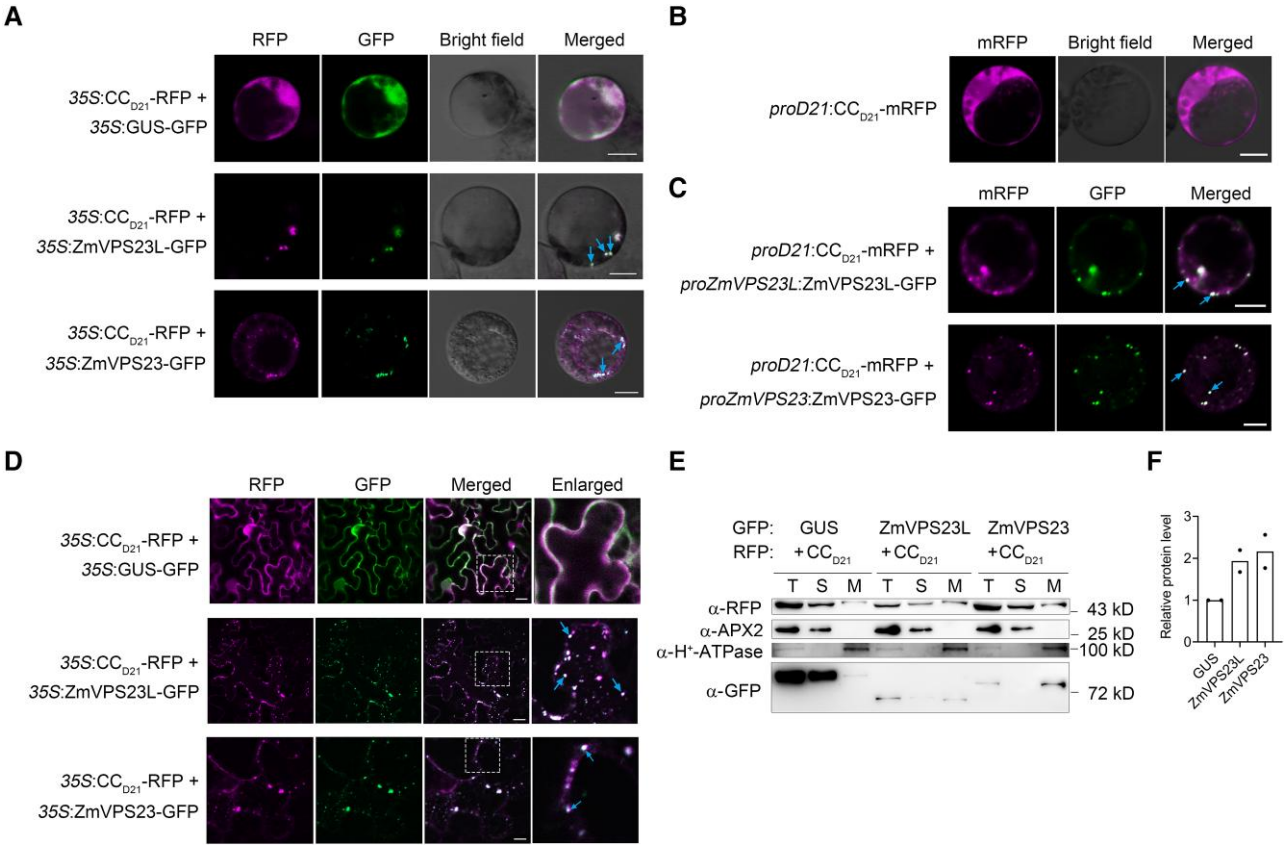

Figure 6. ZmVPS23L and ZmVPS23 change the subcellular localization of CC_{D21} in maize protoplasts and *N. benthamiana* leaves. **A)** *ZmVPS23L-GFP* and *ZmVPS23-GFP* driven by the 35S promoter were transiently co-expressed with *CC_{D21}-mRFP* in maize protoplasts. *GUS-GFP* was used as control. Arrows indicate the colocalization of ZmVPS23L or ZmVPS23 with CC_{D21}. Scalce bars, 10 μm. **B)** *CC_{D21}-mRFP* driven by the *Rp1-D21* promoter was transiently expressed in maize protoplasts. Scale bars, 10 μm. **C)** *ZmVPS23L-GFP* and *ZmVPS23-GFP* were transiently co-expressed with *CC_{D21}- mRFP* under their native promoters in maize protoplasts. Arrows indicate the colocalization of ZmVPS23L or ZmVPS23 with CC_{D21}. Scale bars, 10 μm. **D)** *ZmVPS23L-EGFP* and *ZmVPS23 -EGFP* driven by the 35S promoter were transiently co-expressed with *CC_{D21}-mRFP* in *N. benthamiana*. *GUS-EGFP* was used as control. Images in the white boxes are enlarged and shown in the right panel. Arrows indicate the colocalization of ZmVPS23L or ZmVPS23 with CC_{D21}. Scale bars, 10 μm. **E)** Protein fractionation assay. *ZmVPS23L-EGFP* and *ZmVPS23-EGFP* driven by the 35S promoter were transiently co-expressed with *CC_{D21}-mRFP* in *N. benthamiana*. *GUS-EGFP* was used as control. Total protein (T), soluble (S), and microsomal (M) fraction were extracted 30 hai. APX2 and H^+-ATPase were used as soluble and microsomal fraction markers, respectively. **F)** Quantification of the CC_{D21} in microsomal fractions (M in Fig. 6E). The quantitation of the CC_{D21}-RFP bands in microsomal fractions was normalized to the quantitation of the H^+-ATPase band in the same sample. The normalized microsomal CC_{D21}-RFP when co-expressed with *GUS* was set to 1.0. The values are calculated from data of two repetitions.

play important roles in biotic and abiotic stresses, in addition to regulating NLR-mediated HR.

ZmVPS23L acts like VPS23 in affecting the protein sorting of the NLR protein Rp1-D21

Phylogenetic analysis indicated that ZmVPS23L and ZmVPS23 were homologous to At2g38830 and AtVPS23 in *Arabidopsis*, respectively (Fig. 4A). As the key component in ESCRT-I that is involved in protein sorting and vesicle trafficking, AtVPS23 has multiple functions in cytokinesis, salt stress, and ABA signaling (Spitzer et al. 2006; Yu et al. 2016; Lou et al. 2020). AtVPS23 was reported to interact with the ABA receptors PYR1/PYLs and sort them into vacuoles for their degradation (Yu et al. 2016). At2g38830 is homologous to AtVPS23A and AtVPS23B; however, the function of At2g38830 has not been studied. In maize, ZmVPS23L is phylogenetically close to ZmVPS23, with 20% in amino acid sequence identity, but they harbor similar conserved domains with AtVPS23 and At2g38830 (Supplemental Fig. S9). Therefore, ZmVPS23L and ZmVPS23 might have functions similar to AtVPS23 in protein sorting under biotic and abiotic stresses. According to the subcellular localization, both ZmVPS23L and ZmVPS23 mainly localized in endosomes (Fig. 5 and Supplemental Fig. S11) and colocalized with AtVPS23 (Supplemental Fig. S12). The canonical function of ESCRT components is mainly to sort membrane receptors to the vacuole for degradation (Taelman et al. 2010; Szymanska et al. 2018). ZmVPS23L and ZmVPS23 also interacted with the nucleo-cytoplasmic NLR protein Rp1-D21 and caused its subcellular redistribution, indicating that

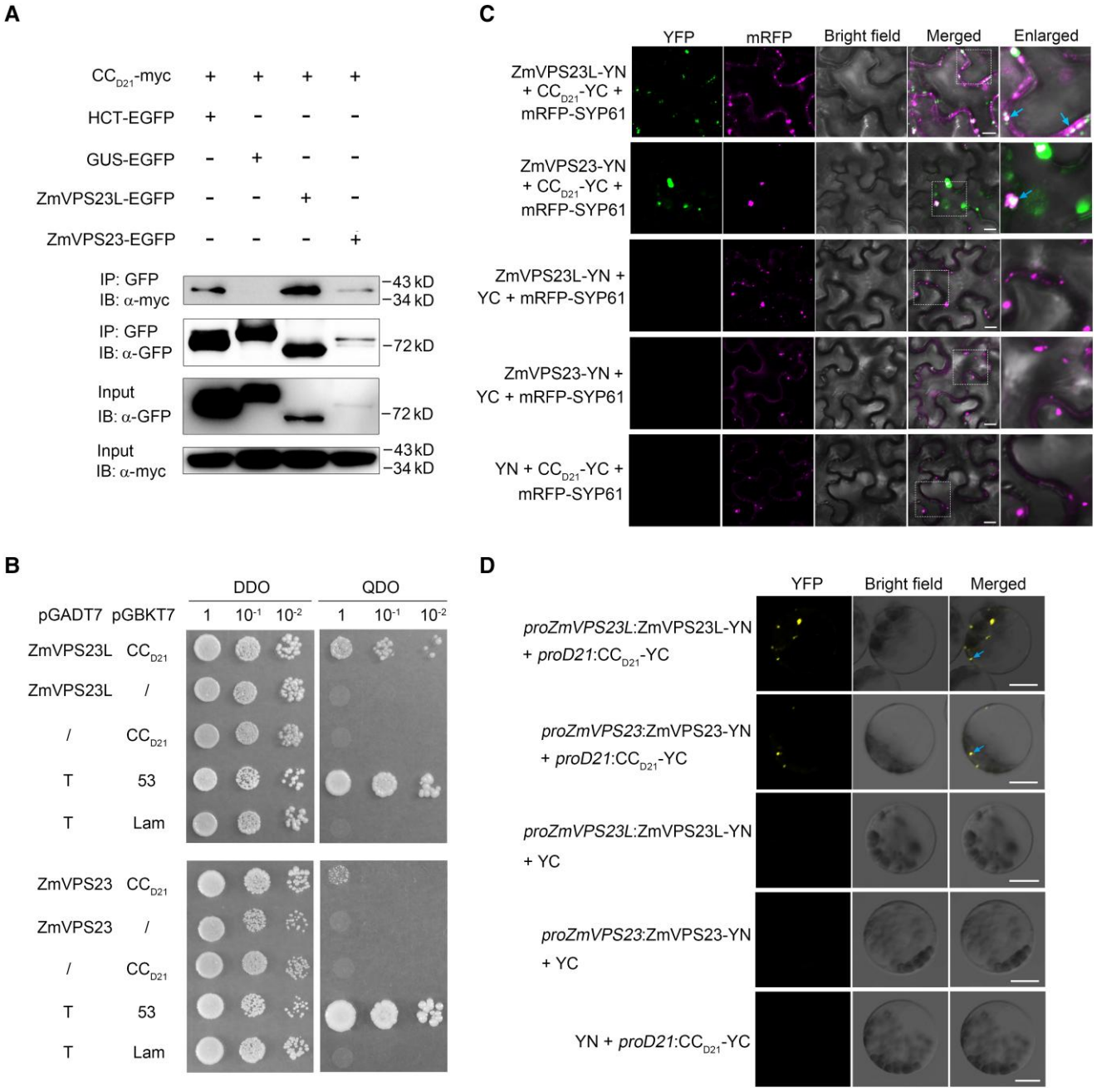

Figure 7. ZmVPS23L and ZmVPS23 interact with the CC$_{D21}$. **A)** Investigating the interaction between ZmVPS23L or ZmVPS23 with CC$_{D21}$ by co-immunoprecipitation (Co-IP) assays. *ZmVPS23L-EGFP* or *ZmVPS23-EGFP* was transiently co-infiltrated with *CC$_{D21}$-c-myc* in *N. benthamiana*. Proteins were extracted at 40 hai. Anti-GFP microbeads were used for immunoprecipitation. Anti-GFP and anti-myc antibodies were used for detection the expression of CC$_{D21}$ and ZmVPS23L/ZmVPS23 proteins, respectively. *GUS-EGFP* and *HCT-EGFP* were used as negative and positive controls, respectively. **B)** Investigating the interaction between ZmVPS23L or ZmVPS23 with CC$_{D21}$ by yeast two-hybrid assays. T + 53 and T + Lam were used as positive and negative controls, respectively. **C)** Investigating the interaction between ZmVPS23L or ZmVPS23 with CC$_{D21}$ by bimolecular fluorescence complementation (BiFC) assays in *N. benthamiana*. Constructs encoding ZmVPS23L and ZmVPS23 fused to the N terminus of YFP (YN) driven by the 35S promoter, and *CC$_{D21}$* driven by the 35S promoter was cloned in-frame upstream of *YFP* (*YC*). *CC$_{D21}$-YC* was transiently co-infiltrated with *ZmVPS23L-YN* or *ZmVPS23-YN*, and endosome marker m*RFP-SYP61* in *N. benthamiana*. Confocal images were taken at 36 hai. Arrows indicate the colocalization of the punctate signals with endosome marker. Scale bars, 10 μm. **D)** Investigating the interaction between ZmVPS23L and ZmVPS23 with CC$_{D21}$ under their native promoters by BiFC assays in maize protoplasts. Constructs encoding ZmVPS23L and ZmVPS23 were fused to the N terminus of YFP (YN) driven by their native promoters, and CC$_{D21}$ was fused to the C terminus of YFP (YC) and driven by its native promoter. The above BiFC vectors were transiently co-transfected in maize protoplasts. Arrows indicate the punctate signals. Scale bars, 10 μm.

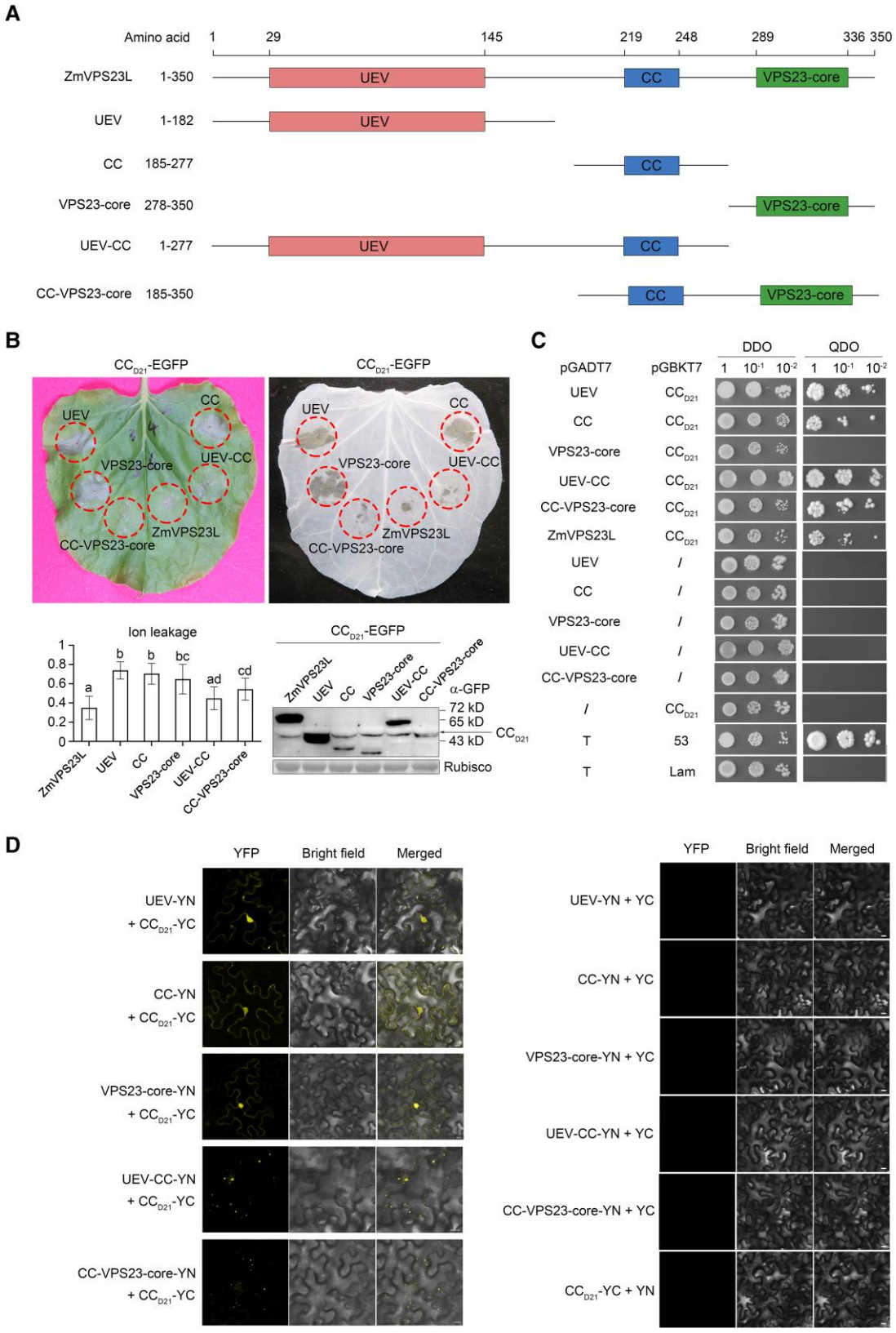

Figure 8. The UEV-CC domain and CC-VPS23 core domain of ZmVPS23L partially suppresses CC$_{D21}$-mediated HR in *N. benthamiana*. **A)** Schematic diagram of the ZmVPS23L domain architecture and the fragments used for HR analysis. The amino acid positions of the different domains are shown on the top and the position of fragments are shown on the left. **B)** HR phenotype when *CC$_{D21}$* was transiently co-expressed with different

(continued)

ZmVPS23L and ZmVPS23 also act in protein sorting. Unlike the role of AtVPS23A in protein degradation (Yu et al. 2016), ZmVPS23L and ZmVPS23 did not appear to affect the protein accumulation of Rp1-D21 (Figs. 1B and 4B).

The ESCRT complex has been reported to be involved in plant immunity in several studies. For instance, the ESCRT-I component AtVPS37 affects PTI by interacting with the PRR FLS2 and mediating the sorting of FLS2. Both AtVPS37 and AtVPS28 are essential for resistance to *Pto* DC3000 (Spallek et al. 2013). A recent study showed that the ESCRT-0 component NbTOL9a is targeted by the oomycete effector AVRcap1b and is required for suppressing the HR mediated by the helper NLR NRC3 (NLR protein required for hypersensitive response (HR)–associated cell death 3) in *N. benthamiana* (Derevnina et al. 2021). However, the underlying mechanism of how ESCRT components regulate NLR-mediated defense response remains unknown. In this study, we revealed that ZmVPS23 and ZmVPS23L were negative regulators of HR mediated by the CC-NLR protein Rp1-D21, but not by the other two CC-NLRs MLA10 or RPM1(D502). We further showed that ZmVPS23 and ZmVPS23L interacted with CC_{D21}, but not CC_{MLA}, suggesting that the physical interaction between ZmVPS23 or ZmVPS23L with CC_{D21} was required for HR suppression, representing a new mechanism by which ESCRT components regulate NLR-mediated defense response in plants. Further work is needed to determine if this mechanism is specific to Rp1-D and related NLRs or if it is of more general importance.

ZmVPS23L might sequester Rp1-D21 in the endosomes to block autoimmune signal transduction

The appropriate subcellular localization of NLR proteins is important for HR induction. For instance, potato (*Solanum tuberosum*) CC-NLR R3a is in the cytoplasm in its "resting" state. R3a relocates to the late endosome after activation by its cognate effector Avr3a (from *P. infestans*), and this endosome distribution is essential for HR induction (Engelhardt et al. 2012). The tomato (*Solanum lycopersicum*) PRR SlEIX2 (ethylene-inducing xylanase 2) is important for PTI induced by the fungal PAMP ethylene-inducing xylanase (EIX). EIX can trigger the endosomal localization of SlEIX2 (Bar and Avni 2009; Sharfman et al. 2011). Interestingly, the CNL protein SlNRC4a interacts with SlEIX2 and further induces the endosomal localization of SlEIX2 to function in EIX-mediated defense response (Leibman-Markus et al. 2018). These results indicate that the endosome is an important compartment for plant immunity.

Some NLRs act in plant immunity through changing their subcellular distribution by collaborating with other NLR regulators. For example, the TNL protein suppressor of NPR1-1, constitutive 1 (SNC1) localizes in the nucleus and cytoplasm, and its nuclear localization is required for triggering autoimmunity (Zhu et al. 2010; Xu et al. 2014). Overexpression of the nuclear transport receptor KA120 significantly reduces the nuclear retention of SNC1 and suppresses autoimmunity (Jia et al. 2021). Similarly, the potato NLR protein Sw-5b localizes in the nucleus and cytoplasm, and its different subcellular localizations play different roles in resistance against tospovirus infection (Chen et al. 2021). Importins α and ß interact with Sw-5b. Silencing *importin α* and *importin ß* abolishes the nuclear localization of Sw-5b and the host resistance to tospovirus systemic infection (Chen et al. 2021). Therefore, changing NLR localization can interfere with their function. Rp1-D21 and CC_{D21} mainly localized in the cytoplasm and nucleus, and this nucleo-cytoplasmic distribution is believed to be required for the induction of HR (Wang and Balint-Kurti 2015). In the presence of ZmVPS23L or ZmVPS23 in maize protoplasts or in *N. benthamiana* at native or higher levels, Rp1-D21 and CC_{D21} relocated to endosomes (Fig. 6 and Supplemental Fig. S14). Furthermore, the combination of the UEV domain and the CC domain or the combination of the CC domain and the VPS23 core domain, but not one of its single domains of ZmVPS23L, changed the subcellular localization of CC_{D21} and partially suppressed CC_{D21}-mediated HR (Fig. 8). This result might be due to the intramolecular interaction between different domains of ZmVPS23L, which needs to be investigated in the future. Combined with the results from protein–protein interaction and subcellular localization assays between different domains of ZmVPS23L and CC_{D21}, we propose that both the physical interaction and relocation to endosomes are required for ZmVPS23L to suppress CC_{D21}-mediated HR. We hypothesize that the immune signal transduction between cytoplasm and nucleus is blocked, leading to inhibition of *Rp1-D21*-mediated HR. Therefore, the endosome can also be a compartment sequestering NLR proteins that can otherwise cause detrimental effects to plant cells due to their inappropriate activation.

ZmVPS23L and ZmVPS23 interacted with CC_{D21} and induced its relocation to endosomes (Fig. 7, Supplemental Figs. S14 and S15). Both Rp1-D21 and CC_{D21} can

Figure 8. (Continued)
ZmVPS23L fragments in *N. benthamiana*. The fragments were fused to a C-terminal EGFP tag. The representative photograph was taken at 2 dai. The same leaf cleared with ethanol is shown on the right. Ion leakage conductivity assay was carried out at 42 hai. Significant difference between samples was analyzed using one-way ANOVA with Tukey's honestly significant difference (HSD) test (mean ± SD; $n = 14$, biologically independent leaf discs). Different letters indicate significant differences at $P < 0.05$. Total proteins were extracted from leaves at 30 hai. CC_{D21} and different fragments were detected with an anti-GFP antibody. The arrow indicates the bands of CC_{D21}. Rubisco stained by Coomassie brilliant blue was used for equal loading of samples. **C)** Investigating the interaction between different fragments of ZmVPS23L and CC_{D21} by yeast two-hybrid assay. T + 53 and T + Lam were used as positive and negative controls, respectively. **D)** Investigating the interaction between different fragments of ZmVPS23L and CC_{D21} by BiFC assays in *N. benthamiana*. Different fragments of ZmVPS23L were fused to the N terminus of YFP (YN), and CC_{D21} was fused to the C terminus of YFP (YC). Confocal images were taken at 36 hai. Scale bars, 10 μm. The experiments were performed three times with similar results.

self-associate (Wang et al. 2015b). ZmVPS23L and ZmVPS23 also formed homomers and heteromers (Supplemental Fig. S17). We speculate that the self-association of ZmVPS23L might tend to promote some Rp1-D21/ZmVPS23L/ZmVPS23 complexes to form oligomers. Intriguingly, co-expression of *ZmVPS23L* and CC_{D21} in *N. benthamiana* led to aggregation and the formation of some condensates of sizes that were larger than endosomes (Supplemental Movie S1 online). ZmVPS23L and ZmVPS23 might act to recruit Rp1-D21 to condensates or as a scaffold to connect other Rp1-D21 regulators with Rp1-D21 in the condensates, which can sequester Rp1-D21 from the original nucleocytoplasmic localization and suppress HR (Fig. 9).

NLR proteins need to be finely controlled by intra- and intermolecular interactions. Several types of NLR regulators have been identified, including E3 ligases, kinases, transcriptional factors, and molecular chaperones (Sun et al. 2021). Here, we characterized the NLR regulator ZmVPS23L, which interacted with CC_{D21} and changed its subcellular localization to negatively modulate Rp1-D21-mediated HR. Recently, the cryo-electron microscopy structure of at least four plant resistosomes have been characterized: the CC-NLRs ZAR1 (HOPZ-activated resistance 1) and Sr35, the TIR-NLR proteins RPP1 (recognition of *Peronospora parasitica* 1) and ROQ1 (recognition of XopQ 1) (Wang et al. 2019; Ma et al. 2020; Martin et al. 2020; Förderer et al. 2022; Zhao et al. 2022). Among them, the pentameric ZAR1 resistosome containing ZAR1 and the two other host regulators RKS1 (resistance-related kinase 1) and uridylylated PBL2 (AVRPPHB susceptible 1-like 2) act as a calcium-permeable cation channel for NLR activation (Wang et al. 2019; Bi et al. 2021). Since the effectors have not been identified, we have no evidence to support whether ZmVPS23L/ZmVPS23 can form a putative resistosome with Rp1-D21 or other Rp1 proteins. In the absence of pathogen, we propose that ZmVPS23L and ZmVPS23 might form a preactivation complex with Rp1-D21 and likely with other Rp1 proteins predominantly in the endosomes in the resting state. In the presence of pathogens, the transcript levels of genes encoding Rp1 proteins are likely induced to trigger HR. The transcript levels of *ZmVPS23L* and *ZmVPS23* are also presumably induced to restrict the spreading of HR. Another possibility calls upon the targeting of ZmVPS23L/ZmVPS23 or their unidentified adaptors by putative effectors and therefore reduces the interaction between ZmVPS23L or ZmVPS23 and Rp1 proteins to release Rp1 proteins or changes the conformation of the complex for activation (Fig. 9). The knowledge learned here will lay the basis for further investigating the molecular mechanism of VPS23L and VPS23 in plant immunity.

Materials and methods

Plasmid construction

All primers used in this study are listed in Supplemental Table S1. All maize genes used in this study were cloned from the maize (*Zea mays*) inbred line B73 unless otherwise noted. To generate maize overexpressing lines, the coding sequence of *ZmVPS23L* was cloned into the pXG071 vector, which was derived from the pCAMBIA3301 vector, by adding the maize aleurone layer–specific promoter to drive the expression of the *DsRed2* fluorescent marker to distinguish positive and negative transgenic seeds by eye. For transient expression in maize protoplasts, the *ZmVPS23L* and *ZmVPS23* coding sequences were cloned into a modified pUC19 vector with a *GFP* sequence; CC_{D21}-*mRFP* was generated in our previous study (Luan et al. 2021). For transient expression in *N. benthamiana*, pSITEII-N1-EGFP and pSITEII-N1-TaqRFP vectors with the cauliflower mosaic virus (CaMV) 35S promoter (Martin et al. 2009) were used. For subcellular localization in maize protoplasts, *proZmVPS23L*:*ZmVPS23L-GFP* and *proZmVPS23*:*ZmVPS23-GFP* were individually generated by digesting the modified pBI221 vector containing *GFP* with *Pst* I and *BamH* I to replace the 35S promoter with the native promoters of *ZmVPS23L* or *ZmVPS23*. The *proD21*:CC_{D21}-*GFP* construct was generated by digesting a modified pBI221 vector containing *RFP* with *Hind* III and *Spe* I to replace the 35S promoter with the native promoter of CC_{D21}. For BiFC assay with native promoters in maize protoplasts, *proZmVPS23L*:*ZmVPS23L-YN*, *proZmVPS23*:*ZmVPS23-YN*, and *proD21*:CC_{D21}-*YC* were individually generated by digesting the pVYNE(R) or pVYCE(R) vectors (Waadt et al. 2008; Xu et al. 2022) with *Hind* III and *Xba* I to replace the 35S promoter with the native promoters from *ZmVPS23L*, *ZmVPS23*, or CC_{D21}.

Plant materials and growth conditions

Rp1-D21 was maintained in a heterozygous state in the A632 background (A632:*Rp1-D21*) since homozygous *Rp1-D21* mutant plants are sterile. B104:*Rp1-D21* was obtained by crossing the inbred line B104 with pollen from the A632:*Rp1-D21* mutant. *ZmVPS23L* was transformed into the donor line B104. For phenotypic analysis, two homozygous T2 lines overexpressing *ZmVPS23L* and their nontransgenic siblings were crossed to B104:*Rp1-D21*. F1 seedlings carrying *Rp1-D21* derived from the cross between *ZmVPS23L*-OE lines and *Rp1-D21* mutants were self-pollinated to generate F2 populations. The homozygous mutant line for *ZmVPS23L* carrying an *Ac/Ds* transposon insertion was obtained from the maize stock center (maizeGDB) and crossed to A632:*Rp1-D21*. The F1 plants carrying *Rp1-D21* were subsequently backcrossed twice to the homozygous line of *Zmvps23l* to obtain a BC2F1 population. The F1, F2, and BC2F1 seedlings were planted in the field of Qingdao, China, in mid-May. For subcellular localization, B73 maize seedlings were grown in darkness at 24°C until the two-leaf stage. *N. benthamiana* seedlings were planted at 24°C under a 16-h light (90 μmol m^{-2} s^{-1} provided by white LEDs)/8-h dark cycle.

RT-qPCR analysis

Total RNA was extracted from leaves of maize seedlings at the five-leaf stage using RNAiso reagent (Takara,

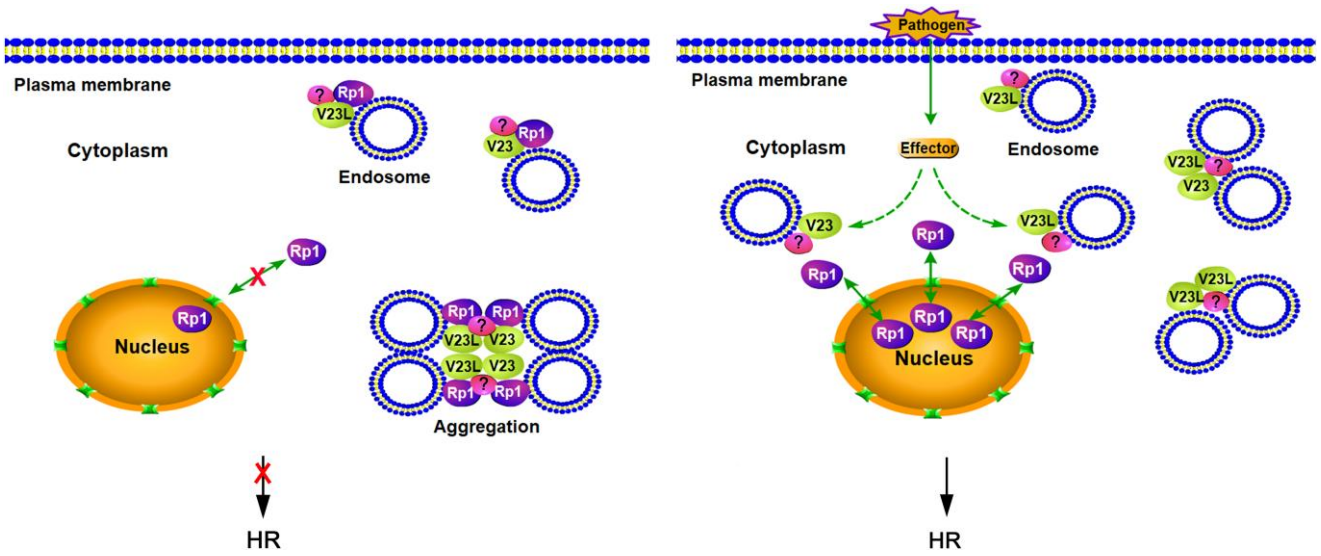

Figure 9. The working models for elucidating the mechanisms of ZmVPS23L in suppression of *Rp1-D21*-mediated HR. The nucleo-cytoplasmic trafficking of Rp1-D21 induces HR in plant cells (Wang and Balint-Kurti 2016). ZmVPS23L and ZmVPS23 form homomers and heteromers. In the absence of pathogen, ZmVPS23L and ZmVPS23 interact with the CC_{D21} domain and relocates Rp1-D21 to endosomes. Some endosomes carrying Rp1-D21 and ZmVPS23L further fused and formed protein aggregations. Relocation of Rp1-D21 blocks its nucleo-cytoplasmic trafficking and suppresses *Rp1-D21*-mediated HR. In the presence of pathogen, putative effectors might target ZmVPS23L and ZmVPS23 or their adaptors and reduce the interaction between ZmVPS23L and ZmVPS23 and Rp1 proteins to release Rp1 proteins or change the conformation of the complex for activation.

http://www.takara.com.cn). Reverse transcription was carried out using HiScript III RT SuperMix for qPCR (Vazyme, http://www.vazyme.com) following the manufacturer's instructions. qPCR analysis was performed with a qTOWER^{3}G real-time PCR system (Analytik Jena) using SYBR qPCR Mix (Vazyme), and *ZmActin* was used as the reference gene. The data were calculated using the $2^{-\triangle\triangle CT}$ method (Livak and Schmittgen 2001). Primer sequences are listed in Supplemental Table S1.

Assessment of chlorophyll content

One hundred milligrams of maize leaves was ground and mixed with 1 mL 80% (v/v) acetone and 5 mg $CaCO_3$ in 2 mL tubes. The ground mixture was kept in darkness for 12 h and centrifuged at 12,000 rpm for 5 min at 4°C; then 200 µL of the supernatant was taken to measure the absorbance at 645 and 663 nm. The total content of chlorophyll (mg g^{-1}) was calculated by the following formula (Su et al. 2010):

$$\text{Chlorophyll content} = (20.31A_{645} + 8.05A_{663}) \times V(1000 \times W)$$

with V being the volume of the extraction solvent (mL) and W the fresh weight of the sample (g).

Transient expression in *N. benthamiana*

Agrobacterium (*Agrobacterium tumefaciens*)-mediated transient expression was performed as previously described (Wang et al. 2015a). Briefly, *Agrobacterium* strain GV3101 (with pMP90) transformed with different binary vectors were cultured in LB medium at 28°C overnight and resuspended in resuspension buffer (10 mM $MgCl_2$, 10 mM MES pH 5.6, 200 µM acetosyringone). The agrobacteria were placed at room temperature for 3 h and then infiltrated into the leaves of 4-week-old *N. benthamiana*. Unless otherwise stated, all experiments were performed at least three times with similar results.

Ion leakage assay

The procedures were performed as described in our previous study (Wang et al. 2015b). At least 15 individual leaves of *N. benthamiana* were infiltrated, and at least 4 leaves from different plants were collected for ion leakage assay. Unless otherwise stated, all experiments were performed at least three times with similar results.

Transient expression in maize protoplasts

Mesophyll protoplasts were isolated from maize inbred line B73 or *ZmVPS23L* overexpression lines and transfected using the polyethylene glycol (PEG) method according to the protocols reported previously (Sheen 1991; Yoo et al. 2007). Briefly, the middle part of the second leaves of etiolated maize seedlings was cut into thin strips and digested with enzyme solution (1.5% [w/v] cellulase RS, 0.3% [w/v] macerozyme R10, 0.6 M mannitol, 10 mM MES pH 5.7, 1 mM $CaCl_2$). Released protoplasts were washed with W5 solution and resuspended with MMg solution (Sheen 1991; Yoo et al. 2007) to a final cell density of 2×10^5/mL. One hundred microliters of protoplasts was mixed with 10 to 20 µg

plasmids and 100 µL PEG solution. The mixture was incubated for 30 min and washed with W5 solution.

Confocal microscopy

Confocal images were taken at 40 h after transient expression in *N. benthamiana* and 24 h after transient expression in maize protoplasts on a laser scanning confocal microscope (LSM 880, Zeiss). EGFP was excited at 488 nm, and its emission was collected between 495 and 550 nm. RFP was excited at 561 nm with its emission collected between 580 and 675 nm. The excitation wavelength of YFP was 514 nm with its emission collected between 520 and 570 nm.

Protein extraction and Co-IP assay

Protein extraction and Co-IP assays were carried out as described in a previous study (Wang et al. 2015a). Briefly, for protein extraction, three leaf discs with a diameter of 1.2 cm were collected from different leaves at 30 h after infiltration (hai) in *N. benthamiana*. Total protein was extracted from ground samples using 150 µL protein extraction buffer (20 mM Tris-HCl pH 8.0, 150 mM NaCl, 1 mM EDTA pH 8.0, 1% [v/v] Triton X-100, 0.1% [w/v] SDS, 10 mM DTT, 40 µM MG132 and 1× plant protein protease inhibitor mixture [Sigma-Aldrich]). For Co-IP assay, 0.6 g of samples from three different leaves was collected at 40 hai in *N. benthamiana*. Protein was extracted using 1.8 mL extraction buffer (50 mM HEPES pH 7.5, 50 mM NaCl, 10 mM EDTA pH 8.0, 0.5% [v/v] Triton X-100, 4 mM DTT, 40 µM MG132, and 1× plant protein protease inhibitor mixture [Sigma-Aldrich]). Co-IP was performed using a kit (130-091-125, Miltenyi Biotec) following the manufacturer's instructions. The immunoblot assays were performed based on our previous studies (Wang et al. 2015b). For GFP detection, anti-GFP (GenScript, Cat# A01704) was used at a dilution of 1:6,000, and an anti-rabbit-HRP second antibody (GenScript, Cat# A00098) was used at a dilution of 1:5,000. For myc detection, anti-myc (GenScript, Cat# Cat# A00704) was used at a dilution of 1:5,000, and an anti-mouse HRP second antibody (GenScript, Cat# A00160) was used at a dilution of 1:5,000.

Microsomal fractionation

Microsomal fractionation assays were carried out as described in a previous study (Wang and Balint-Kurti 2015) with minor modifications. About 1.5 g of leaves collected from infiltrated *N. benthamiana* was ground in liquid nitrogen and mixed with 6 mL cold lysis buffer (50 mM Tris-HCl pH 7.5, 0.33 M sucrose, 150 mM NaCl, 1 mM EDTA, 10 mM DTT, 20 µM MG132, and 1 × protein protease inhibitor cocktail). The homogenate was centrifuged at 5000 × *g* for 10 min at 4°C. The supernatant was filtered through one layer of Miracloth and a 100 µL aliquot was set aside as total protein (T). The remaining supernatant was centrifuged at 100,000 × *g* for 1 h at 4°C. The supernatant was collected and designated as the soluble fraction (S). The pellet was washed with lysis buffer twice and resuspended in 900 µL lysis buffer and designated as microsomal fraction (M). The extracted proteins were subsequently analyzed by immunoblotting. Primary antibodies used for microsomal fractionation assays were anti-RFP (1:2,000, Rockland, Cat# 600401379), anti-APX2 (1:2,500, Abmart, PHO5419), anti-H^+-ATPase (1:5,000, Agrisera, AS07260), and anti-GFP (1:6,000, GenScript, Cat# A01704). An anti-rabbit HRP second antibody (GenScript, Cat# A00098) was used at a dilution of 1:5,000.

Yeast two-hybrid assay

ZmVPS23L and ZmVPS23 were constructed into pGADT7 vector and CC_{D21} into pGBKT7 vector (Clontech). Different vectors were co-transformed into yeast strain Y2HGold and selected on double dropout (DDO) (synthetic defined [SD]—Trp–Leu) medium and quadruple dropout QDO (SD–Trp–Leu–His–Ade) medium.

Yeast protein abundance analysis

To analyze the protein abundance of bait and prey proteins for yeast two-hybrid assays, the yeast strain Y2HGold containing pGADT7 or pGBKT7 constructs was grown overnight in SD–Leu medium or SD–Trp medium, respectively. The cultures were pelleted when the OD600 reached about 1.0. The pellet was mixed with 200 µL 2 M NaOH and incubated on ice for 10 min. Then, 200 µL 50% (w/v) trichloroacetic acid (TCA) was added, and the mixture was incubated on ice for 2 h. The mixture was centrifuged at 14,000 × g for 20 min at 4°C. The pellet was mixed with 200 µL acetone and centrifuged at 14,000 × g for 20 min at 4°C. The pellet was resuspended with 200 µL 5% (w/v) SDS and then mixed with 200 µL SDS sample buffer (25 mM Tris-HCl pH 6.8, 9 M urea, 1 mM EDTA, 1% [w/v] SDS, 0.7 M β-mercaptoethanol, and 10% [v/v] glycerol). To each sample, 2 M Tris-HCl (pH 9.0) was added until the color of the samples changed from yellow to blue. The samples were incubated at 37°C for 15 min, centrifuged at 14,000 × g for 5 min, and analyzed by immunoblotting. The pGADT7 constructs and pGBKT7 constructs were detected by α-HA and α-myc antibodies, respectively.

BiFC assay

The *ZmVPS23L*, *ZmVPS23*, and CC_{D21} coding sequences were cloned into YN and YC vectors derived from split yellow fluorescent protein. Different YN- and YC-derived vectors were co-infiltrated in *N. benthamiana*. Images were taken at 48 hai using confocal microscopy (LSM 880, Carl Zeiss).

Phylogenetic analysis

ZmVPS23L was used as a query to search the National Center for Biotechnology Information (NCBI) database for its homologs from different species. The alignment of ZmVPS23L and its homologs was performed using ClustalW. The phylogenetic tree was generated using the neighbor-joining method with 1,000 bootstrap replicates by MEGA5 (Tamura et al. 2011). The alignment and tree files are provided as Supplemental Files S1 and S2.

Accession numbers

Sequence data of genes cloned from maize can be found in the Maize Genetics and Genomics Database (https://maizegdb.org/) under the following accession numbers: *ZmVPS23L* (GRMZM2G109582), *ZmVPS23* (GRMZM2G147579), *Hsp70* (GRMZM2G001500), *POLA* (GRMZM2G059010), *8695* (GRMZM2G348695), *1989* (AC198929.2_FG002).

Acknowledgments

We are grateful to Drs. Liwen Jiang, Qi Xie, and Yan Zhang for kindly providing the endosome markers SYP61, VSR2, and ARA7, Dr. Shi Xiao for providing *mCherry:AtVPS23A*, and Dr. Caiji Gao for providing the pBI221-derived vector for maize protoplasts assays. We thank Haiyan Yu, Xiaomin Zhao, and Sen Wang from SKLMT (State Key Laboratory of Microbial Technology, Shandong University) for the assistance in microimaging and LSCM analysis. We thank Dr. Peter Balint-Kurti for critical reading and helpful discussions on the manuscript.

Author contributions

G.-F.W. conceived the experiments. Y.S. performed the experiments. S.M. and X.L. helped analyze the data. Y.S. and G.-F.W wrote the manuscript.

Supplemental data

The following materials are available in the online version of this article.

Supplemental Figure S1. *ZmVPS23L* does not change plant height when overexpressed.

Supplemental Figure S2. ZmVPS23L suppresses Rp1-D21-mediated HR in maize F2 populations.

Supplemental Figure S3. The *Zmvps23l* mutant used in this study.

Supplemental Figure S4. Genotyping of a BC2F1 population by PCR.

Supplemental Figure S5. Sequence alignment of the promoter regions of *ZmVPS23L* from Mo17 and different NAM parental lines.

Supplemental Figure S6. Relative transcript levels of *ZmVPS23L* and *PR1* in NAM parental lines containing *Rp1-D21* as determined by RT-qPCR.

Supplemental Figure S7. Amino acid sequence alignment of ZmVPS23L from Mo17 and different NAM parental lines.

Supplemental Figure S8. ZmVPS23L from Mo17 and different NAM parental lines have no obvious difference in suppressing CC_{D21}-EGFP-mediated HR in *N. benthamiana*.

Supplemental Figure S9. Amino acid sequence alignment of ZmVPS23L and its homologs in maize and Arabidopsis.

Supplemental Figure S10. ZmVPS23L and ZmVPS23 do not suppress cell death induced by other CC-NLRs and elicitors.

Supplemental Figure S11. Subcellular localization of ZmVPS23L and ZmVPS23 in *N. benthamiana* leaves and maize protoplasts.

Supplemental Figure S12. ZmVPS23L and ZmVPS23 colocalize with AtVPS23A in *N. benthamiana* leaves and maize protoplasts.

Supplemental Figure S13. ZmVPS23L and ZmVPS23 do not colocalize with the ER marker, Golgi marker or peroxisome marker.

Supplemental Figure S14. ZmVPS23L and ZmVPS23 change the subcellular localization of Rp1-D21.

Supplemental Figure S15. ZmVPS23L promotes the localization of CC_{D21} to endosomes.

Supplemental Figure S16. ZmVPS23L and ZmVPS23 do not interact with the CC domain of MLA10.

Supplemental Figure S17. ZmVPS23L and ZmVPS23 form homomers and heteromers.

Supplemental Figure S18. The combination of the UEV domain and CC domain of ZmVPS23L changes the subcellular localization of CC_{D21} in *N. benthamiana*.

Supplemental Figure S19. Protein abundance tests for yeast two-hybrid assays.

Supplemental Figure S20. Protein abundance tests for BiFC assays.

Supplemental Table S1. List of primers used in this study.

Supplemental File S1. Alignment of protein sequences used for the phylogenetic tree shown in Fig. 4A.

Supplemental File S2. Newick format of the phylogenetic tree.

Supplemental Movie online 1. Confocal microscopy movie showing the dynamics of the formation of large protein aggregates when CC_{D21}:mRFP and ZmVPS23L:EGFP were co-expressed in *N. benthamiana*.

Funding

This research was supported by grants from the National Natural Science Foundation of China (31871944, 32072405, and 31801370), the National Key Research and Development Program of China (2022YFD1201802), and the Key R&D Project of Shandong Province (2021LZGC022).

Conflict of interest statement. None declared.

Data availability

All relevant data are available in the manuscript and the supplementary material of this article.

References

Bai S, Liu J, Chang C, Zhang L, Maekawa T, Wang Q, Xiao W, Liu Y, Chai J, Takken FLW, et al. Structure-function analysis of barley NLR immune receptor MLA10 reveals its cell compartment specific activity in cell death and disease resistance. PLoS Pathog. 2012:**8**(6): e1002752. https://doi.org/10.1371/journal.ppat.1002752

Balint-Kurti P. The plant hypersensitive response: concepts, control and consequences. Mol Plant Pathol. 2019:**20**(8): 1163–1178. https://doi.org/10.1111/mpp.12821

Bar M, Avni A. EHD2 inhibits ligand-induced endocytosis and signaling of the leucine-rich repeat receptor-like protein LeEix2. Plant J. 2009:**59**(4): 600–611. https://doi.org/10.1111/j.1365-313X.2009.03897.x

Bent AF, Mackey D. Elicitors, effectors, and R genes: the new paradigm and a lifetime supply of questions. Annu Rev Phytopathol. 2007:**45**(1): 399–436. https://doi.org/10.1146/annurev.phyto.45.062806.094427

Bi G, Su M, Li N, Liang Y, Dang S, Xu J, Hu M, Wang J, Zou M, Deng Y, et al. The ZAR1 resistosome is a calcium-permeable channel triggering plant immune signaling. Cell. 2021:**184**(13):3528–3541.e12. https://doi.org/10.1016/j.cell.2021.05.003

Bomblies K, Weigel D. Hybrid necrosis: autoimmunity as a potential gene-flow barrier in plant species. Nat Rev Genet. 2007:**8**(5): 382–393. https://doi.org/10.1038/nrg2082

Cesari S, Moore J, Chen C, Webb D, Periyannan S, Mago R, Bernoux M, Lagudah ES, Dodds PN. Cytosolic activation of cell death and stem rust resistance by cereal MLA-family CC–NLR proteins. Proc Natl Acad Sci U S A. 2016:**113**(36): 10204–10209. https://doi.org/10.1073/pnas.1605483113

Chakraborty J, Ghosh P, Das S. Autoimmunity in plants. Planta. 2018:**248**(4): 751–767. https://doi.org/10.1007/s00425-018-2956-0

Chen H, Qian X, Chen X, Yang T, Feng M, Chen J, Cheng R, Hong H, Zheng Y, Mei Y, et al. Cytoplasmic and nuclear Sw-5b NLR act both independently and synergistically to confer full host defense against tospovirus infection. New Phytol. 2021:**231**(6): 2262–2281. https://doi.org/10.1111/nph.17535

Chintamanani S, Hulbert SH, Johal GS, Balint-Kurti PJ. Identification of a maize locus that modulates the hypersensitive defense response, using mutant-assisted gene identification and characterization. Genetics. 2010:**184**(3): 813–825. https://doi.org/10.1534/genetics.109.111880

Christie N, Myburg AA, Joubert F, Murray SL, Carstens M, Lin Y-C, Meyer J, Crampton BG, Christensen SA, Ntuli JF, et al. Systems genetics reveals a transcriptional network associated with susceptibility in the maize–grey leaf spot pathosystem. Plant J. 2017:**89**(4): 746–763. https://doi.org/10.1111/tpj.13419

Dangl JL, Jones JDG. Plant pathogens and integrated defence responses to infection. Nature. 2001:**411**(6839): 826–833. https://doi.org/10.1038/35081161

Deng Y, Zhai K, Xie Z, Yang D, Zhu X, Liu J, Wang X, Qin P, Yang Y, Zhang G, et al. Epigenetic regulation of antagonistic receptors confers rice blast resistance with yield balance. Science. 2017:**355**(6328): 962–965. https://doi.org/10.1126/science.aai8898

Derevnina L, Contreras MP, Adachi H, Upson J, Cruces AV, Xie RR, Sklenar J, Menke FLH, Mugford ST, MacLean D, et al. Plant pathogens convergently evolved to counteract redundant nodes of an NLR immune receptor network. Plos Biol. 2021:**19**(8): e3001136. https://doi.org/10.1371/journal.pbio.3001136

Ding Y, Murphy KM, Poretsky E, Mafu S, Yang B, Char SN, Christensen SA, Saldivar E, Wu M, Wang Q, et al. Multiple genes recruited from hormone pathways partition maize diterpenoid defences. Nat Plants. 2019:**5**(10): 1043–1056. https://doi.org/10.1038/s41477-019-0509-6

Engelhardt S, Boevink PC, Armstrong MR, Ramos MB, Hein I, Birch PR. Relocalization of late blight resistance protein R3a to endosomal compartments is associated with effector recognition and required for the immune response. Plant Cell. 2012:**24**(12): 5142–5158. https://doi.org/10.1105/tpc.112.104992

Förderer A, Li E, Lawson AW, Deng Y-N, Sun Y, Logemann E, Zhang X, Wen J, Han Z, Chang J, et al. A wheat resistosome defines common principles of immune receptor channels. Nature. 2022:**610**-(7932):532–539. https://doi.org/10.1038/s41586-022-05231-w

Gao Z, Chung E-H, Eitas TK, Dangl JL. Plant intracellular innate immune receptor resistance to *Pseudomonas syringae* pv. maculicola 1 (RPM1) is activated at, and functions on, the plasma membrane. Proc Natl Acad Sci U S A. 2011:**108**(18): 7619–7624. https://doi.org/10.1073/pnas.1104410108

Gao C, Zhuang X, Shen J, Jiang L. Plant ESCRT complexes: moving beyond endosomal sorting. Trends Plant Sci. 2017:**22**(11): 986–998. https://doi.org/10.1016/j.tplants.2017.08.003

Gatta AT, Carlton JG. The ESCRT-machinery: closing holes and expanding roles. Curr Opin Cell Biol. 2019:**59**: 121–132. https://doi.org/10.1016/j.ceb.2019.04.005

Ge C, Wang Y-G, Lu S, Zhao XY, Hou B-K, Balint-Kurti PJ, Wang G-F. Multi-omics analyses reveal the regulatory network and the function of ZmUGTs in maize defense response. Front Plant Sci. 2021:**12**: 738261. https://doi.org/10.3389/fpls.2021.738261

Hu G, Richter TE, Hulbert SH, Pryor T. Disease lesion mimicry caused by mutations in the rust resistance gene rp1. Plant Cell. 1996:**8**(8): 1367–1376. https://doi.org/10.2307/3870307

Hulbert SH. Structure and evolution of the rp1 complex conferring rust resistance in maize. Annu Rev Phytopathol. 1997:**35**(1): 293–310. https://doi.org/10.1146/annurev.phyto.35.1.293

Jia M, Shen X, Tang Y, Shi X, Gu Y. A karyopherin constrains nuclear activity of the NLR protein SNC1 and is essential to prevent autoimmunity in *Arabidopsis*. Mol Plant. 2021:**14**(10):1733–1744. https://doi.org/10.1016/j.molp.2021.06.011

Jones JD, Dangl JL. The plant immune system. Nature. 2006:**444**(7117): 323–329. https://doi.org/10.1038/nature05286

Kamoun S, van West P, Vleeshouwers VGAA, de Groot KE, Govers F. Resistance of *Nicotiana benthamiana* to *Phytophthora infestans* is mediated by the recognition of the elicitor protein INF1. Plant Cell. 1998:**10**(9): 1413–1425. https://doi.org/10.1105/tpc.10.9.1413

Kourelis J, van der Hoorn RAL. Defended to the nines: 25 years of resistance gene cloning identifies nine mechanisms for R protein function. Plant Cell. 2018:**30**(2): 285–299. https://doi.org/10.1105/tpc.17.00579

Lacomme C, Santa Cruz S. Bax-induced cell death in tobacco is similar to the hypersensitive response. Proc Natl Acad Sci U S A. 1999:**96**(14): 7956–7961. https://doi.org/10.1073/pnas.96.14.7956

Leibman-Markus M, Pizarro L, Schuster S, Lin ZJD, Gershony O, Bar M, Coaker G, Avni A. The intracellular nucleotide binding leucine-rich repeat receptor - SlNRC4a enhances immune signaling elicited by extracellular perception. Plant Cell Environ. 2018:**41**(10): 2313–2327. https://doi.org/10.1111/pce.13347

Liu G, Liang J, Lou L, Tian M, Zhang X, Liu L, Zhao Q, Xia R, Wu Y, Xie Q, et al. The deubiquitinases UBP12 and UBP13 integrate with the E3 ubiquitin ligase XBAT35.2 to modulate VPS23A stability in ABA signaling. Sci Adv. 2022:**8**(14): eabl5765. https://doi.org/10.1126/sciadv.abl5765

Livak KJ, Schmittgen TD. Analysis of relative gene expression data using real-time quantitative PCR and the $2-\Delta\Delta CT$ method. Methods. 2001:**25**(4): 402–408. https://doi.org/10.1006/meth.2001.1262

Lou L, Yu F, Tian M, Liu G, Wu Y, Wu Y, Xia R, Pardo JM, Guo Y, Xie Q. ESCRT-I component VPS23A sustains salt tolerance by strengthening the SOS module in *Arabidopsis*. Mol Plant. 2020:**13**(8): 1134–1148. https://doi.org/10.1016/j.molp.2020.05.010

Luan Q-L, Zhu Y-X, Ma S, Sun Y, Liu X-Y, Liu M, Balint-Kurti PJ, Wang G-F. Maize metacaspases modulate the defense response mediated by the NLR protein Rp1-D21 likely by affecting its subcellular localization. Plant J. 2021:**105**(1): 151–166. https://doi.org/10.1111/tpj.15047

Ma S, Lapin D, Liu L, Sun Y, Song W, Zhang X, Logemann E, Yu D, Wang J, Jirschitzka J, et al. Direct pathogen-induced assembly of an NLR immune receptor complex to form a holoenzyme. Science. 2020:**370**(6521):eabe3069. https://doi.org/10.1126/science.abe3069

Martin K, Kopperud K, Chakrabarty R, Banerjee R, Brooks R, Goodin MM. Transient expression in *Nicotiana benthamiana* fluorescent marker lines provides enhanced definition of protein localization, movement and interactions in plants. Plant J. 2009:**59**(1): 150–162. https://doi.org/10.1111/j.1365-313X.2009.03850.x

Martin R, Qi T, Zhang H, Liu F, King M, Toth C, Nogales E, Staskawicz BJ. Structure of the activated ROQ1 resistosome directly recognizing the pathogen effector XopQ. Science (New York, N.Y.). 2020:**370**(6521): eabd9993. https://doi.org/10.1126/science.abd9993

Murphree C, Kim S-B, Karre S, Samira R, Balint-Kurti P. Use of virus-induced gene silencing to characterize genes involved in modulating hypersensitive cell death in maize. Mol Plant Pathol. 2020:**21**-(12): 1662–1676. https://doi.org/10.1111/mpp.12999

Negeri A, Wang G-F, Benavente L, Kibiti CM, Chaikam V, Johal G, Balint-Kurti P. Characterization of temperature and light effects on the defense response phenotypes associated with the maize Rp1-D21autoactive resistance gene. BMC Plant Biol. 2013:**13**(1): 106. https://doi.org/10.1186/1471-2229-13-106

Ngou BPM, Ahn H-K, Ding P, Jones JDG. Mutual potentiation of plant immunity by cell-surface and intracellular receptors. Nature. 2021:**592**(7852): 110–115. https://doi.org/10.1038/s41586-021-03315-7

Olukolu BA, Negeri A, Dhawan R, Venkata BP, Sharma P, Garg A, Gachomo E, Marla S, Chu K, Hasan A, et al. A connected set of genes associated with programmed cell death implicated in controlling the hypersensitive response in maize. Genetics. 2013:**193**(2): 609–620. https://doi.org/10.1534/genetics.112.147595

Olukolu BA, Wang G-F, Vontimitta V, Venkata BP, Marla S, Ji J, Gachomo E, Chu K, Negeri A, Benson J, et al. A genome-wide association study of the maize hypersensitive defense response identifies genes that cluster in related pathways. PLoS Genet. 2014:**10**(8): e1004562. https://doi.org/10.1371/journal.pgen.1004562

Otegui MS. ESCRT-mediated sorting and intralumenal vesicle concatenation in plants. Biochem Soc Trans. 2018:**46**(3): 537–545. https://doi.org/10.1042/BST20170439

Padmanabhan MS, Ma S, Burch-Smith TM, Czymmek K, Huijser P, Dinesh-Kumar SP. Novel positive regulatory role for the SPL6 transcription factor in the N TIR-NB-LRR receptor-mediated plant innate immunity. PLoS Pathog. 2013:**9**(3): e1003235. https://doi.org/10.1371/journal.ppat.1003235

Qi D, Innes RW. Recent advances in plant NLR structure, function, localization, and signaling. Front Immunol. 2013:**4**: 348. https://doi.org/10.3389/fimmu.2013.00348

Qi T, Seong K, Thomazella DPT, Kim JR, Pham J, Seo E, Cho M-J, Schultink A, Staskawicz BJ. NRG1 functions downstream of EDS1 to regulate TIR-NLR-mediated plant immunity in *Nicotiana benthamiana*. Proc Natl Acad Sci U S A. 2018:**115**(46): E10979–E10987. https://doi.org/10.1073/pnas.1814856115

Richardson L, Howard A, Khuu N, Gidda S, McCartney A, Morphy B, Mullen R. Protein–protein interaction network and subcellular localization of the *Arabidopsis thaliana* ESCRT machinery. Front Plant Sci. 2011:**2**:20. https://doi.org/10.3389/fpls.2011.00020

Sharfman M, Bar M, Ehrlich M, Schuster S, Melech-Bonfil S, Ezer R, Sessa G, Avni A. Endosomal signaling of the tomato leucine-rich repeat receptor-like protein LeEix2. Plant J. 2011:**68**(3): 413–423. https://doi.org/10.1111/j.1365-313X.2011.04696.x

Sheen J. Molecular mechanisms underlying the differential expression of maize pyruvate, orthophosphate dikinase genes. Plant Cell. 1991:**3**(3): 225–245. https://doi.org/10.1105/tpc.3.3.225

Smith SM, Steinau M, Trick HN, Hulbert SH. Recombinant Rp1 genes confer necrotic or nonspecific resistance phenotypes. Mol Genet Genomics. 2010:**283**(6): 591–602. https://doi.org/10.1007/s00438-010-0536-5

Spallek T, Beck M, Ben Khaled S, Salomon S, Bourdais G, Schellmann S, Robatzek S. ESCRT-I mediates FLS2 endosomal sorting and plant immunity. PLoS Genet. 2013:**9**(12): e1004035. https://doi.org/10.1371/journal.pgen.1004035

Spitzer C, Schellmann S, Sabovljevic A, Shahriari M, Keshavaiah C, Bechtold N, Herzog M, Müller S, Hanisch F-G, Hülskamp M. The *Arabidopsis* elch mutant reveals functions of an ESCRT component in cytokinesis. Development. 2006:**133**(23): 4679–4689. https://doi.org/10.1242/dev.02654

Su S, Zhou Y, Qin JG, Yao W, Ma Z. Optimization of the method for chlorophyll extraction in aquatic plants. J Freshwater Ecol. 2010:**25**(4): 531–538. https://doi.org/10.1080/02705060.2010.9664402

Sun Q, Collins NC, Ayliffe M, Smith SM, Drake J, Pryor T, Hulbert SH. Recombination between paralogues at the rp1 rust resistance locus in maize. Genetics. 2001:**158**(1): 423–438. https://doi.org/10.1093/genetics/158.1.423

Sun H, Zhu X, Li C, Ma Z, Han X, Luo Y, Yang L, Yu J, Miao Y. Xanthomonas effector XopR hijacks host actin cytoskeleton via complex coacervation. Nat Commun. 2021:**12**(1): 4064. https://doi.org/10.1038/s41467-021-24375-3

Szymanska E, Budick-Harmelin N, Miaczynska M. Endosomal "sort" of signaling control: the role of ESCRT machinery in regulation of receptor-mediated signaling pathways. Semin Cell Dev Biol. 2018:**74**: 11–20. https://doi.org/10.1016/j.semcdb.2017.08.012

Taelman VF, Dobrowolski R, Plouhinec J-L, Fuentealba LC, Vorwald PP, Gumper I, Sabatini DD, De Robertis EM. Wnt signaling requires sequestration of glycogen synthase kinase 3 inside multivesicular endosomes. Cell. 2010:**143**(7): 1136–1148. https://doi.org/10.1016/j.cell.2010.11.034

Tamura K, Peterson D, Peterson N, Stecher G, Nei M, Kumar S. MEGA5: molecular evolutionary genetics analysis using maximum likelihood, evolutionary distance, and maximum parsimony methods. Mol Biol Evol. 2011:**28**(10): 2731–2739. https://doi.org/10.1093/molbev/msr121

Waadt R, Schmidt LK, Lohse M, Hashimoto K, Bock R, Kudla J. Multicolor bimolecular fluorescence complementation reveals simultaneous formation of alternative CBL/CIPK complexes in plants. Plant J. 2008:**56**(3): 505–516. https://doi.org/10.1111/j.1365-313X.2008.03612.x

Wang G-F, Balint-Kurti PJ. Cytoplasmic and nuclear localizations are important for the hypersensitive response conferred by maize autoactive Rp1-D21 protein. Mol Plant-Microbe Interact. 2015:**28**(9): 1023–1031. https://doi.org/10.1094/MPMI-01-15-0014-R

Wang G-F, Balint-Kurti PJ. Maize homologs of CCoAOMT and HCT, two key enzymes in lignin biosynthesis, form complexes with the NLR rp1 protein to modulate the defense response. Plant Physiol. 2016:**171**(3): 2166–2177. https://doi.org/10.1104/pp.16.00224

Wang G-F, He Y, Strauch R, Olukolu BA, Nielsen D, Li X, Balint-Kurti PJ. Maize homologs of hydroxycinnamoyltransferase, a key enzyme in lignin biosynthesis, bind the nucleotide binding leucine-rich repeat rp1 proteins to modulate the defense response. Plant Physiol. 2015a:**169**(3): 2230–2243. https://doi.org/10.1104/pp.15.00703

Wang J, Hu M, Wang J, Qi J, Han Z, Wang G, Qi Y, Wang HW, Zhou JM, Chai J. Reconstitution and structure of a plant NLR resistosome conferring immunity. Science. 2019:**364**(6435):eaav5870. https://doi.org/10.1126/science.aav5870

Wang GF, Ji J, El-Kasmi F, Dangl JL, Johal G, Balint-Kurti PJ. Molecular and functional analyses of a maize autoactive NB-LRR protein identify precise structural requirements for activity. PLoS Pathog. 2015b:**11**(2): e1004674. https://doi.org/10.1371/journal.ppat.1004674

Xia F-N, Zeng B, Liu H-S, Qi H, Xie L-J, Yu L-J, Chen Q-F, Li J-F, Chen Y-Q, Jiang L, et al. SINAT E3 ubiquitin ligases mediate FREE1 and VPS23A degradation to modulate abscisic acid signaling. Plant Cell. 2020:**32**(10): 3290–3310. https://doi.org/10.1105/tpc.20.00267

Xu F, Cheng YT, Kapos P, Huang Y, Li X. P-loop-dependent NLR SNC1 can oligomerize and activate immunity in the nucleus. Mol Plant. 2014:**7**(12): 1801–1804. https://doi.org/10.1093/mp/ssu097

Xu Y, Wang Y, Du J, Pei S, Guo S, Hao R, Wang D, Zhou G, Li S, O'Neill M, et al. A DE1 BINDING FACTOR 1–GLABRA2 module regulates rhamnogalacturonan I biosynthesis in Arabidopsis seed coat mucilage. Plant Cell. 2022:**34**(4): 1396–1414. https://doi.org/10.1093/plcell/koac011

Yoo S-D, Cho Y-H, Sheen J. Arabidopsis mesophyll protoplasts: a versatile cell system for transient gene expression analysis. Nat Protoc. 2007:**2**(7): 1565–1572. https://doi.org/10.1038/nprot.2007.199

Yu F, Cao X, Liu G, Wang Q, Xia R, Zhang X, Xie Q. ESCRT-I component VPS23A is targeted by E3 ubiquitin ligase XBAT35 for proteasome-

mediated degradation in modulating ABA signaling. Mol Plant. 2020:**13**(11): 1556–1569. https://doi.org/10.1016/j.molp.2020.09.008

Yu F, Lou L, Tian M, Li Q, Ding Y, Cao X, Wu Y, Belda-Palazon B, Rodriguez PL, Yang S, et al. ESCRT-I component VPS23A affects ABA signaling by recognizing ABA receptors for endosomal degradation. Mol Plant. 2016:**9**(12): 1570–1582. https://doi.org/10.1016/j.molp.2016.11.002

Yu Y, Zhang H, Long Y, Shu Y, Zhai J. Plant public RNA-seq database: a comprehensive online database for expression analysis of ~45 000 plant public RNA-seq libraries. Plant Biotechnol J. 2022:**20**(5): 806–808. https://doi.org/10.1111/pbi.13798

Yuan M, Jiang Z, Bi G, Nomura K, Liu M, Wang Y, Cai B, Zhou J-M, He SY, Xin X-F. Pattern-recognition receptors are required for NLR-mediated plant immunity. Nature. 2021:**592**(7852): 105–109. https://doi.org/10.1038/s41586-021-03316-6

Zhao Y-B, Liu M-X, Chen T-T, Ma X, Li Z-K, Zheng Z, Zheng S-R, Chen L, Li Y-Z, Tang L-R, et al. Pathogen effector AvrSr35 triggers Sr35 resistosome assembly via a direct recognition mechanism. Sci Adv. 2022:**8**(36): eabq5108. https://doi.org/10.1126/sciadv.abq5108

Zhu Y, Qian W, Hua J. Temperature modulates plant defense responses through NB-LRR proteins. PLoS Pathog. 2010:**6**(4): e1000844. https://doi.org/10.1371/journal.ppat.1000844